moz regulates Hox expression and pharyngeal segmental identity in zebrafish

Craig T. Miller*,†, Lisa Maves and Charles B. Kimmel

Institute of Neuroscience, 1254 University of Oregon, Eugene, OR 97403, USA

*Present address: Department of Developmental Biology, 279 Campus Drive, Beckman Center B300, Stanford University School of Medicine, Stanford, CA 94305, USA
†Author for correspondence (ctm@stanford.edu)

Summary

In vertebrate embryos, streams of cranial neural crest (CNC) cells migrate to form segmental pharyngeal arches and differentiate into segment-specific parts of the facial skeleton. To identify genes involved in specifying segmental identity in the vertebrate head, we screened for mutations affecting cartilage patterning in the zebrafish larval pharynx. We present the positional cloning and initial phenotypic characterization of a homeotic locus discovered in this screen. We show that a zebrafish ortholog of the human oncogenic histone acetyltransferase MOZ (monocytic leukemia zinc finger) is required for specifying segmental identity in the second through fourth pharyngeal arches. In *moz* mutant zebrafish, the second pharyngeal arch is dramatically transformed into a mirror-image duplicated jaw. This phenotype resembles a similar but stronger transformation than that seen in hox2 morpholino oligo (hox2-MO) injected animals. In addition, mild anterior homeotic transformations are seen in the third and fourth pharyngeal arches of *moz* mutants. *moz* is required for maintenance of most *hox1-4* expression domains and this requirement probably at least partially accounts for the *moz* mutant homeotic phenotypes. Homeosis and defective Hox gene expression in *moz* mutants is rescued by inhibiting histone deacetylase activity with Trichostatin A.

Although we find early patterning of the *moz* mutant hindbrain to be normal, we find a late defect in facial motoneuron migration in *moz* mutants. Pharyngeal musculature is transformed late, but not early, in *moz* mutants. We detect relatively minor defects in arch epithelia of *moz* mutants. Vital labeling of arch development reveals no detectable changes in CNC generation in *moz* mutants, but later prechondrogenic condensations are mispositioned and misshapen.

Mirror-image *hox2*-dependent gene expression changes in postmigratory CNC prefigure the homeotic phenotype in *moz* mutants. Early second arch ventral expression of *goosecoid* (*gsc*) in *moz* mutants and in animals injected with hox2-MOs shifts from lateral to medial, mirroring the first arch pattern. *bapx1*, which is normally expressed in first arch postmigratory CNC prefiguring the jaw joint, is ectopically expressed in second arch CNC of *moz* mutants and hox2-MO injected animals. Reduction of *bapx1* function in wild types causes loss of the jaw joint. Reduction of *bapx1* function in *moz* mutants causes loss of both first and second arch joints, providing functional genetic evidence that *bapx1* contributes to the *moz*-deficient homeotic pattern. Together, our results reveal an essential embryonic role and a crucial histone acetyltransferase activity for Moz in regulating Hox expression and segmental identity, and provide two early targets, *bapx1* and *gsc*, of *moz* and *hox2* signaling in the second pharyngeal arch.

Introduction

The jaw forms embryonically as hinged dorsal and ventral cartilages in the first (mandibular) pharyngeal arch. The jaw cartilages are classically considered segmentally homologous with the jaw-supporting cartilages in the second (hyoid) pharyngeal arch and the gill-supporting (branchial) cartilages in more posterior pharyngeal arches (Kimmel et al., 2001b). First arch cranial neural crest (CNC), which forms the jaw, lacks Hox gene expression. Second and more posterior arch CNC displays a nested pattern of Hox gene expression (Hunt et al., 1991). *Hox2* genes act as selector genes for second arch segmental identity: mutation of *Hoxa2* in the mouse or reduction of *hoxa2b* and *hoxb2a* function in zebrafish results in homeotic transformation of second pharyngeal arch skeletal

elements into first arch identity (Gendron-Maguire et al., 1993; Rijli et al., 1993; Hunter and Prince, 2002) (C. T. Miller, PhD Thesis, University of Oregon, 2001). Downregulation of *Hoxa2* expression by ectopic sources of FGF8 results in a similar transformation of the second arch-derived skeletal elements in the chick (Trainor et al., 2002). Forcing ectopic expression of *Hoxa2* in the first arch of *Xenopus* or chicks, or *hoxa2b* and *hoxb2a* in zebrafish, results in the converse phenotype, where the jaw segment adopts a second arch morphology (Grammatopoulos et al., 2000; Pasqualetti et al., 2000; Hunter and Prince, 2002). Other Hox genes are proposed to specify segmental identity throughout the pharyngeal arches (Hunt et al., 1991). In support of this, ectopic expression of *Hoxa2* can divert the *Xenopus* third pharyngeal arch (the first

gill-bearing or branchial arch) towards hyoid fate (Pasqualetti et al., 2000). Furthermore, third arch CNC in *valentino* (*val*) mutant zebrafish inappropriately expresses *hoxb2a*, which is normally restricted to second arch CNC, perhaps contributing to a mild transformation of the *val* mutant third arch cartilages to a second arch pattern (Moens et al., 1998; Kimmel et al., 2001a).

Although it is still not clear why *Hox2* dysfunction results in homeotic transformations, analyses in the mouse, chick and *Xenopus* have begun to unravel the *Hox2*-responsive genetic circuitry. A subtractive screen in mice discovered that *Pitx1* is ectopically expressed in *Hoxa2* mutant second arch primordia, and inactivating *Pitx1* in a *Hoxa2* mutant partially rescues the homeosis (Bobola et al., 2003). Expression analyses in mice reveal that at late stages *Hoxa2* represses expression of the chondrogenic factor *Sox9* and the osteogenic factor *Runx2* (*Cbfa1*) (Kanzler et al., 1998). Two other known *Hoxa2* target genes are the homeobox genes *bapx1* and *goosecoid* (*gsc*). In *Xenopus*, ectopic expression of *Hoxa2* in the first arch represses expression of *Bapx1* (Pasqualetti et al., 2000). In chicks, ectopic expression of *Hoxa2* induces *Gsc* expression (Grammatopoulos et al., 2000), and in zebrafish early *gsc* expression is reported to be downregulated in hox2-MO injected animals (Hunter and Prince, 2002). Both *Gsc* and *bapx1* are essential for craniofacial development, although reducing function of either gene does not result in homeosis (Rivera-Perez et al., 1995; Yamada et al., 1995; Miller et al., 2003).

Hox gene expression is maintained by *trithorax* group (*trx*G) activity, which involves chromatin remodeling, including histone acetylation (Simon and Tamkun, 1998). In humans, mutations in *trx*G members cause leukemia (Look, 1997; Ernst et al., 2002). The MYST family histone acetyltransferase MOZ (monocytic leukemia zinc finger protein; MYST3 – Human Gene Nomenclature Database) is mutated in human leukemias (Borrow et al., 1996). Human MOZ is a large protein of 2004 amino acids and biochemical analyses reveal MOZ to possess both histone acetyltransferase (HAT) and transcriptional activation activity (Champagne et al., 2001; Kitabayashi et al., 2001a). Targets of either of these activities in vivo are unknown and the function of MOZ during embryonic development has not been reported.

Previous screens in zebrafish have identified a large number of mutations causing craniofacial defects (Schilling et al., 1996a; Piotrowski et al., 1996; Neuhauss et al., 1996). The cloning of several of these mutations [*endothelin1* (*edn1* or *sucker*) (Miller et al., 2000); *tbx1* (*van gogh*) (Piotrowski et al., 2003); *tf2ap2a* (*lockjaw*) (Knight et al., 2003)] reveals remarkable conservation in the genetic control of vertebrate craniofacial development, as each of these molecules is also required for patterning the mammalian pharyngeal arches (Kurihara et al., 1994; Jerome and Papaioannou, 2001; Schorle et al., 1996; Zhang et al., 1996). To identify genes required for segmental identity in the pharyngeal arches, we directly screened for mutations affecting cartilage patterning in zebrafish.

We present the molecular identification and phenotypic characterization of a zebrafish homeotic mutant discovered in this screen. Fine mapping, positional cloning, sequencing and morpholino phenocopy experiments reveal this homeotic locus to encode a zebrafish ortholog of the human oncogene MOZ, a MYST family HAT. Severely reduced *hox2* expression in *moz* mutant zebrafish contributes to a mirror-image duplication of

jaw cartilages in place of second arch cartilages. *moz* is also more broadly required for maintenance of most *hox1-4* expression domains, probably resulting in the homeotic transformation of the third and fourth arch gill support cartilages. In the hindbrain, *moz* is required for maintenance, but not initiation, of Hox gene expression, and *moz* mutants display aberrant facial motoneuron migration. Inhibition of histone deacetylase activity with Trichostatin A rescues Hox maintenance defects and homeotic cartilage transformations in *moz* mutants, indicating that HAT activity is essential for *moz* function. Pharyngeal musculature appears transformed late but not early in *moz* mutants. We find little evidence for patterning defects in arch epithelia of *moz* mutants. However, striking gene expression changes in *moz* mutant postmigratory hyoid CNC are apparent. Expression of *bapx1*, which is normally restricted to the jaw joint (Miller et al., 2003) is robustly duplicated in second arch CNC of *moz* mutants. Although reduction of *bapx1* function in wild-type embryos results in absence of the jaw joint (Miller et al., 2003), reduction of *bapx1* function results in absence of both the first and second arch joints in *moz* mutants. Expression of *gsc* is profoundly reorganized in the *moz* mutant second arch, with lateral CNC expression shifting to medial, mirroring the wild-type first arch pattern. Together our results reveal that a zebrafish ortholog of the human oncogene *MOZ* regulates Hox gene expression and segmental identity in the vertebrate pharynx.

Materials and methods

Fish maintenance and Alcian screen

Fish were raised and staged as described (Westerfield, 1995; Kimmel et al., 1995). For the head cartilage screen, ENU-mutagenized F2 gynogenetic diploid clutches were generated by EP treatment (Streisinger et al., 1981). Mutagenesis was postmeiotic (Riley and Grunwald, 1995) for *b719* and premeiotic (Solnica-Krezel et al., 1994) for *b999*. Survivors at day four were fixed, stained with Alcian Green, and bleached to remove pigmentation as described (Miller et al., 2003). Clutches were screened for cartilage morphology under a Zeiss STEMI SR dissecting microscope at 50× magnification. The recessive larval lethal mutations *b719* and *b999* were outcrossed to the AB strain. All detailed phenotypic analyses were carried out with the *b719* allele.

Mapping and positional cloning

Initial mapping was performed with *moz^b719^* on an outbred *wik* background. Fine mapping was performed with *moz^b719^* crossed onto the *Islet1:GFP* background (Higashijima et al., 2000), which was found to be highly polymorphic relative to AB within the z6371-z7351 interval. In these fish, primers 1 and 2 (Table 1) were used to amplify the microsatellite z6371. Primers and enzymes were used to reveal co-dominant polymorphisms in the 5′ and 3′ UTRs, respectively, of fc32e05 (3+4, *Mnl*I) and fc15g12 (5+6, *Xmn*I). All size polymorphisms were resolved on 1-4% agarose gels using standard techniques. The 3′ end of *mki67l* was not present on PAC74G4. The SP6 end of PAC 14P16 begins with the ninth nucleotide of the fc15g12 ORF. PAC ends were sequenced and the following primers and enzymes used to reveal codominant polymorphisms: 4T (T7 end of PAC 4O19, 7+8, *Bcl*I); 14T (T7 end of PAC 14P16, 9+10, *Scf*I); 114T (T7 end of PAC 114E16, 11+12, *Dra*I). Accession numbers are: AY600370 (*moz* cDNA) and CL525848-CL525855 (PAC end sequences).

Phenotypic analyses

In situ hybridization was performed using standard techniques with

Table 1. Primer and morpholino oligo (MO) sequences

Primer/MO	Sequence (5′ to 3′)
1	GCCTGGCATTTTAGAAAGCGTTC
2	GAGAGCGCACCTGTACTGG
3	GCTATCTCGCGTCCTAGAAAT
4	CTGCTGAGAGGGAGACAAGTC
5	CATGATTATATTCTTGTATTTCAT
6	CGAGTGCTTGTTTACTGTAGT
7	GAGTGATGCTTCTGCACAAG
8	ACCCTTTGAAGAAGTTGTTG
9	GGGTCAGTCTTAGGCTTAAG
10	AAGGATATAAACAGCTCCAC
11	CCAGTCATCATTGACTCACC
12	ACTACCACAGTACCAGTAAAC
13	GGGAGAGGAGGAACGTAAAGAGGT
14	TGCAAACGGAAGAGGATGGTCCAGAGCTTTG
moz-MO1	<u>CAT</u>GGTTGCTTTAATACTGCTAAGC
moz-MO2	tcatgttgcttacCTGCTGTACTCC
moz-MO3	gagatttcctttcctcacCTCAAAC
hoxa2b-MO	AATTCGTAATT<u>CAT</u>CTCCTCCAAG
hoxb2a-MO	ATTCAAAATT<u>CAT</u>CGCTTCGCCTGG
bapx1-MO	GCGCACAGC<u>CAT</u>GTCGAGCAGCACT

See Materials and methods for description and number of primers. ATG translation start site is underlined for moz-MO1, both hox-MOs and bapx1-MO. For the splice-blocking moz-MOs (MO2 and 3), the intron complementary sequence is in lower case. Although the hoxa2b-MO sequence is identical to that reported in Hunter and Prince (Hunter and Prince, 2002), the hoxb2a-MO sequence we injected was three bases longer than the sequence they report.

PTU-treated animals to inhibit pigmentation (Westerfield, 1995). Genotypes of animals with gene expression defects were confirmed by PCR genotyping, using dCAPS (Neff et al., 1998) to turn the *b719* lesion into a codominant polymorphism (using primers 13+14, followed by cutting with *Bst*XI). Both alleles of *moz* segregate as Mendelian recessive mutations. For all gene expression defects reported for stages before 4 days, at which point the mutant phenotype is readily scorable by morphology, at least four *moz* mutants had their genotypes confirmed by PCR. Embryos and larvae were deyolked manually with an insect pin and eyebrow hair, cleared in 70% glycerol and photographed on a Zeiss Axiophot with Nomarski optics. For motor neuronal analyses, *moz*[b719] heterozygotes were crossed to the *Islet1:GFP* strain (Higashijima et al., 2000). References for probes used are as follows. All Hox probes (Prince et al., 1998); *eng2* (Ekker et al., 1992); *myod* (Weinberg et al., 1996); *α-tropomyosin* (Thisse et al., 1993); *pea3* (Brown et al., 1998); *shh* (Krauss et al., 1993); *pitx2c* (Essner et al., 2000); *rag1* (Willett et al., 1997); *bapx1* (Miller et al., 2003); and *gsc* (Schulte-Merker et al., 1994).

Morpholino oligo injections

MOs were purchased from Gene Tools (Philomath, OR), and sequences are listed in Table 1. MOs were diluted to 25 mg/ml in 1× Danieau buffer. Subsequent dilutions were made in 0.2 M KCl and 0.2% Phenol Red. These dilutions were injected into the yolk of one- to four-cell zebrafish embryos, roughly 5 nl per embryo. hoxa2b-MO and hoxb2a-MO were each injected at 3 mg/ml, and bapx1-MO was injected at 3 mg/ml.

Trichostatin A treatment

Trichostatin A (TSA; Sigma) was dissolved in DMSO to make a 3 mM stock solution, which was stored at –20°C. For embryo incubations, this stock solution was diluted to 0.1 M in Embryo Medium (with 0.003% PTU and penicillin/streptomycin). This concentration of TSA has been shown to cause increased H4 acetylation in zebrafish (Collas et al., 1999); treatments at higher concentrations cause severe edema and severely reduced cartilage

development in wild-type embryos (L.M., unpublished). Embryos in their chorions were incubated in 0.1 M TSA, 0.003% DMSO beginning at 15 hours postfertilization and were maintained in this treatment until fixation for in situ hybridization or Alcian staining. Control sibling embryos were incubated in 0.003% DMSO.

BODIPY labeling

Vital imaging with the fluorescent dye BODIPY-ceramide was performed as described (Yan et al., 2002). Briefly, clutches were soaked in dye continually from late gastrulation onwards. Although animals continue to develop normally in this dye, it does slightly retard development, as does keeping the fish at room temperature, which we did while viewing repeatedly under a Zeiss LSM confocal microscope. Therefore stages given are the corresponding stages at 28°C, based on the head-trunk angle and other morphological criteria (Kimmel et al., 1995). A total of 31 fish were examined, eight mutants and 23 wild-type siblings. One side of the head was imaged from the outer surface to the midline with optical sections 3 μm apart.

Results

A new screen reveals a homeotic locus

Although large scale zebrafish screens revealed over 100 mutations affecting craniofacial development (Schilling et al., 1996a; Piotrowski et al., 1996; Neuhauss et al., 1996), no mutants with clear homeotic pharyngeal arch phenotypes were found. Such phenotypes were possibly to be expected based on homeotic mutant phenotypes in the mouse (Rijli et al., 1993; Gendron-Macguire et al., 1993; Selleri et al., 2001). We reasoned that homeotic phenotypes in fish might not result in a severe overall morphological phenotype and that directly screening pharyngeal cartilage shapes might reveal homeotic loci. We designed a screen in which F2 ENU-mutagenized gynogenetic clutches were grown up to 4 days, and surviving larvae were fixed, stained with Alcian Green to visualize cartilage, and then bleached to remove pigmentation. This enabled rapid scoring of head cartilage shapes under a dissecting microscope. This screen revealed two non-complementing alleles, *b719* and *b999*, of a homeotic locus. We initially named the *b719* locus *bimandibular*, for the apparent homeotic duplication of the first arch (see below).

Positional cloning reveals the homeotic locus to encode *moz*

We mapped *b719* using bulk segregant analysis and subsequent fine mapping to an ~4 cM interval between z7351 and z6371 on LG5 (Fig. 1A, data not shown). Two zebrafish ESTs, fc15g12 and fc32e05, mapped to this region (http://wwwmap.tuebingen.mpg.de; http://134.174.23.167/zonrhmapper/Maps.htm) were found to closely flank the *b719* locus, by 0.11 cM and 0.05 cM, respectively (Fig. 1A). Two PACs for each of these two ESTs were isolated by PCR from DNA pools of an arrayed zebrafish PAC library (Amemiya and Zon, 1999). Mapping polymorphisms derived from the PAC ends revealed that ends of two of the PACs had crossed the recombinants (Fig. 1A). Sequencing the T7 end of PAC4O19 revealed an exon highly homologous to the human histone acetyltransferase *MOZ*, positioning *moz* as within the non-recombinant interval (Fig. 1A). By aligning vertebrate Moz sequences and using degenerate PCR, the rest of the predicted zebrafish *moz* ORF was isolated and is predicted to encode a 2246 amino acid protein. The first five exons were found to
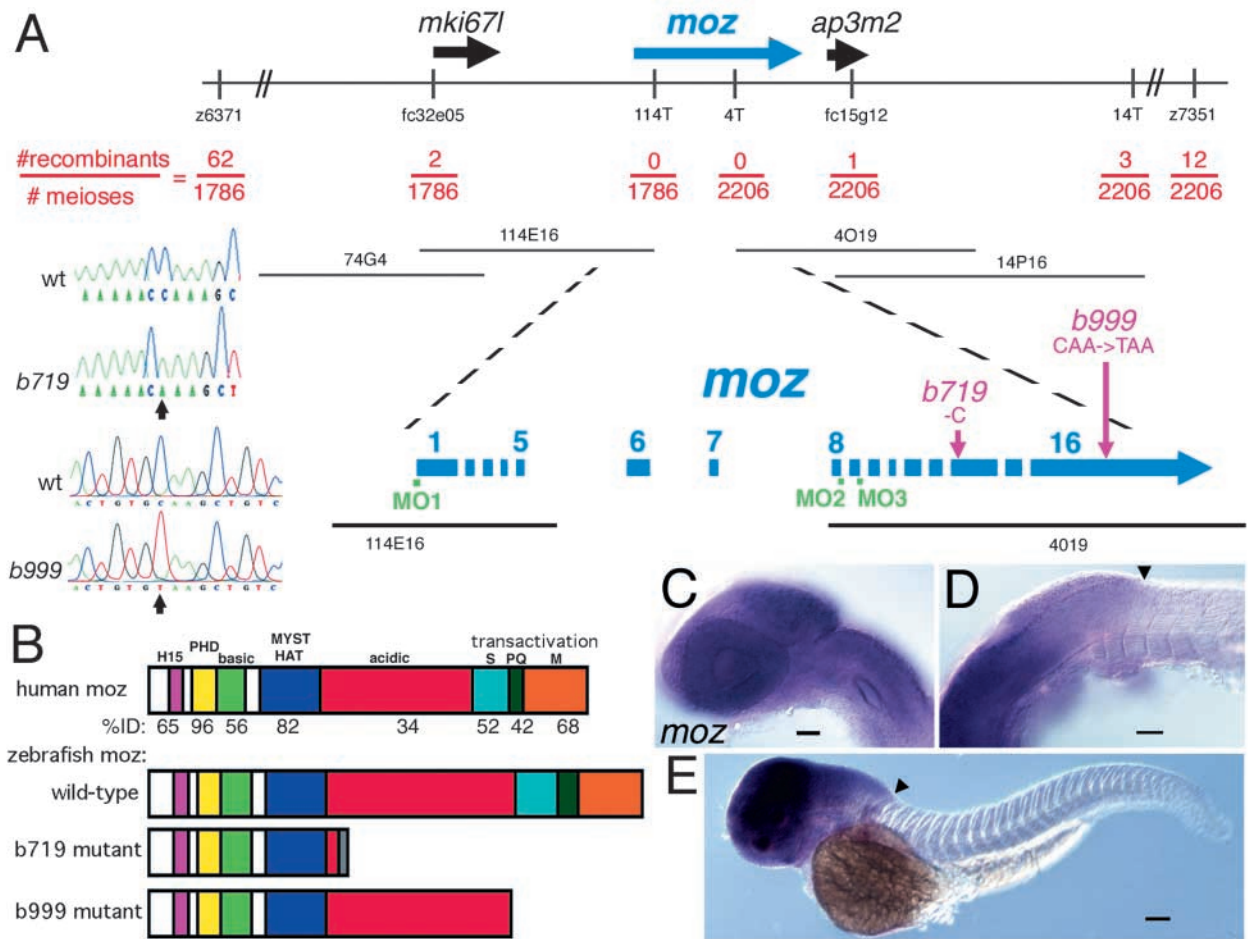
Fig. 1. Mutations in a zebrafish *moz*. (A) Positional cloning of the gene disrupted by the *b719* mutation. The LG5 genomic region is schematized at the top, with informative genetic markers shown. 4T, 14T and 114T are polymorphisms in the T7 end of PACs 4O19, 14P16 and 114E16, respectively. Position of four PACs are shown below the genomic region, with the *moz* region expanded underneath. *moz* spans the non-recombinant interval, with exons on both non-recombinant PAC ends. Lesions are schematized in purple and shown in the chromatograms on the left side of this panel: *b719* deletes one bp (cytosine) in exon 14 of *moz*. A C-to-T missense mutation in *b999* introduces an early stop codon in the 16th exon. Positions of morpholino oligos (MOs) are shown in green (see Tables 1 and 2). (B) Schematic of protein domains of human, zebrafish wild type, *b719* mutant and *b999* mutant. Amino acid domains (Kitabayashi et al., 2001a): H, H15 nuclear localization; PHD, PHD fingers; basic; MYST HAT, MYST family histone acetyltransferase; acidic; serine rich; glutamate rich; methionine rich. The percent identity between human and wild-type zebrafish is listed for each region beneath human MOZ. The C-terminal transactivation domain of human MOZ (Champagne et al., 2001; Kitabayashi et al., 2001a) is labeled. The gray domain in *b719* mutant is frame-shifted prior to translation stop. (C-E) Embryonic expression of *moz* in wild types at 28 hpf (C,D) and 48 hpf (E). Lateral views of head (C), head/trunk interface (D) and whole larva (E). At both stages, *moz* expression appears ubiquitous in cranial tissues, and has a diffuse posterior border of expression near the boundary (arrowhead in D,E) of the hindbrain and spinal cord. Expression at these stages is not detected in the trunk and tail. Scale bars: 50 µm.

reside on PAC 114E16, whereas exons 8-16 were contained on PAC4O19.

Zebrafish Moz is highly conserved with human MOZ (Fig. 1B), a MYST family histone acetyltransferase (HAT, Fig. 1). In addition to activity of its HAT domain, human MOZ contains a transcriptional activation (TA) domain at its C terminus (Champagne et al., 2001; Kitabayashi et al., 2001a). A 1 bp deletion at position 2590 of 6738 in zebrafish *moz*[b719] mutants results in an early frameshift, predicted to produce a truncated protein lacking this TA domain (Fig. 1A,B). A C-to-T nonsense mutation at position 4977 of 6738 in *moz*[b999] mutants is predicted to also truncate the TA domain (Fig. 1A,B).

Expression of zebrafish *moz* at 28-48 hours postfertilization

(hpf) appears ubiquitous in the head but expression is undetectable in the trunk and tail (Fig. 1C-E). The diffuse posterior boundary of *moz* expression during this time frame roughly coincides with the boundary between the hindbrain and spinal cord (Fig. 1C-E). Analyzing *moz* expression at 24, 28, 36 and 48 hpf in clutches of embryos from *moz*[b719] heterozygotes yielded three clear classes of animals based on *moz* expression: strong, intermediate and faint. PCR genotyping revealed the strong class to be homozygous wild types, the intermediate class to be heterozygous for the *moz*[b719] mutation, and the faint class to be *moz*[b719] homozygous mutants. The reduction of *moz* expression in both classes of *moz* mutants appeared to globally affect *moz* expression levels in all cranial tissues (data not shown).

Fig. 2. Homeotic pharyngeal arch phenotype of *moz* mutant larvae. Pharyngeal cartilage phenotypes in wholemounts (A-C) and flat mounts (D-I) of wild-type (A,D,G), *moz* mutant (B,E,H) and moz-MO-injected (C,F,I) larvae at 4 days. (A-F) In *moz* mutants (E) and moz-MO-injected animals (F), both second arch cartilages (M′, pq′) adopt shapes resembling the first arch jaw cartilages. The HM region of HS is deleted (arrow in B). The transformation is incomplete in that the pterygoid process is not seen duplicated in *moz* mutants or moz-MO injected animals. An ectopic dorsal cartilage (arrowhead) is seen in the *moz* mutant third arch. (G-I) Third pharyngeal arch cartilages, with medial to the left. *moz* mutants (H) and moz-MO injected animals (I) display a homeotic third arch phenotype, with a process on their lateral end resembling the retroarticular process on Meckel's cartilage. am, adductor mandibulae; ch, ceratohyal; hm, hyomandibular; hs, hyosymplectic; m, Meckel's; pq, palatoquadrate; ptp, pterygoid process; sy, symplectic. Scale bars: 50 μm.
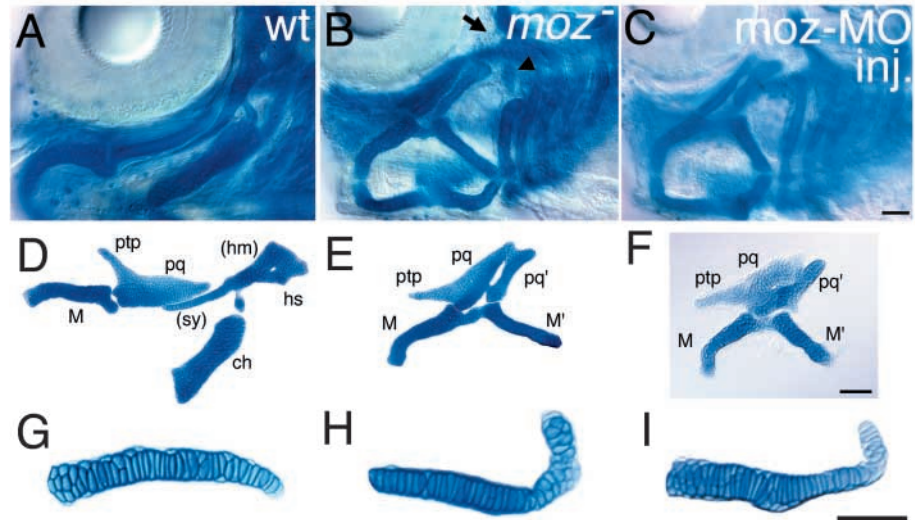
Reducing *moz* function results in pharyngeal cartilage homeosis

In *moz* mutants, second arch cartilages adopt a mirror-image first arch pattern, forming an ectopic jaw (Fig. 2A,B). A novel large opening to the pharynx is present on either side of the head, resembling an ectopic mouth (Fig. 2B, but see below). Especially ventrally, this homeotic phenotype resembles the phenotype seen upon reducing function of both *hoxa2b* and *hoxb2a* (C. T. Miller, PhD Thesis, University of Oregon, 2001) (Hunter and Prince, 2002). Flat-mounting dissected cartilages from *moz* mutants reveals that the second arch cartilages adopt shapes characteristic of first arch cartilages (Fig. 2D,E). In the *moz* mutant second arch, the hyomandibular region of the dorsal second arch cartilage that normally articulates with the otic capsule is missing (Fig. 2D,E; Table 2), presenting a more complete homeotic transformation than observed in the earlier work (C. T. Miller, PhD Thesis, University of Oregon, 2001) (Hunter and Prince, 2002). The *moz* mutant dorsal second arch cartilage, in the more ventral position of the thin symplectic cartilage (Kimmel et al., 1998) is thicker than its wild-type counterpart, resembling the wild-type first arch dorsal (upper) jaw cartilage, the palatoquadrate. The *moz* mutant ventral second arch cartilage is shorter, thinner, contains fewer rows of chondrocytes, and forms a knob on its lateral end, resembling the wild-type first arch ventral (lower) jaw cartilage, Meckel's (Fig. 2; and see below). Furthermore, in the first two arches of *moz* mutants, the dorsal cartilages fuse to one another and the ventral cartilages fuse to one another. by

Table 2. Morpholino oligo phenocopy of the *moz* mutant phenotype

	b719/b719	*b999/b999*	moz-MO1		moz-MO2		moz-MO3	
			5 ng	15 ng	5 ng	15 ng	5 ng	15 ng
n	86	23	41	89	161	55	106	72
% with phenotype (*n*)								
Dorsal deletion	81 (70.0)	22 (5.0)	0 (0.0)	1 (1.0)	0 (0)	0 (0.0)	23 (24.0)	67 (48.5)
Dorsal shape change	100 (86.0)	100 (23.0)	52 (21.5)	86 (76.5)	17 (27.5)	92 (50.5)	93 (98.5)	98 (70.5)
Ventral inversion	99 (85.5)	54 (12.5)	12 (5.0)	29 (26.0)	0 (0.0)	0 (0.0)	44 (40.0)	75 (54.0)
Ventral shape change	100 (86.0)	72 (16.5)	35 (14.5)	60 (53.5)	3 (5.5)	37 (20.5)	86 (91.5)	95 (68.5)
Ventral fusion	98 (84.5)	33 (7.5)	15 (6.0)	19 (17.0)	0 (0.0)	2 (1.0)	41 (43.5)	69 (50.0)
Dorsal fusion	99 (85.5)	44 (10.0)	18 (7.5)	11 (9.5)	0 (0)	33 (18.0)	46 (48.5)	74 (53.5)

Percentage of animals with each phenotype is listed. Of 75 uninjected wild-type control animals, none had any of these six phenotypes (data not shown). The position of each MO is shown in Fig. 1A. For each class, animals were scored on both right and left sides, with each side counting as one-half of an animal. 'Dorsal deletion' includes animals in which no Alcian-positive cartilage articulated with the neurocranium, which in all cases included deletion of the square dorsal half (HM) of HS. 'dorsal shape change' class contains all phenotypes with mispatterned HSs, thus includes the 'HM deletion' class. Other mispatterned HSs include absent foramen, shortening of SY, or other shape changes of HM and/or SY, all of which make HS more simply triangular, resembling its first arch counterpart. 'Ventral inversion' contains animals in which CH, the ventral second arch cartilage, which normally forms a ~45° angle between the lateral side of CH and the midline, makes over a 90° angle between the posterior side of CH and the midline, and branchial cartilage was not deleted. 'Ventral shape change' contains animals in which the second arch ventral cartilage forms an enlarged process on its lateral end (see Fig. 2). In all cases, this second arch ventral cartilage was also smaller and thinner than the wild-type condition, but the presence of the distinctive knob was the criterion for inclusion in this class. 'Ventral fusion' and 'dorsal fusion' contain animals in which the first and second arch ventral and dorsal cartilages were visibly connected with Alcian-positive cartilage. All scoring was made on a high-power dissecting microscope in depigmented and cleared specimens. CH, ceratohyal; HM, hyomandibula; HS, hyosymplectic; SY, symplectic.

contrast, dorsal/ventral fusions within either arch are only rarely seen (see below).

Cartilages in more posterior pharyngeal arches of *moz* mutants are also mispatterned. The third arch ventral cartilage in *moz* mutants appears slightly shorter and thicker and also has a distinctive knob on its lateral end (Fig. 2G,H), resembling the retroarticular process of Meckel's cartilage and thus suggesting a mild transformation of arch three to arch one fate. A similar phenotype is seen in the *moz* mutant fourth arch (data not shown).

To confirm that these homeotic phenotypes in *moz* mutants are due to reduction of Moz function, we injected *moz* morpholino antisense oligonucleotides (MOs). We have previously shown that MO injections can efficiently phenocopy severe phenotypes of larval head skeletal mutants, as well as reveal hypomorphic phenotypes at lower doses (Miller and Kimmel, 2001). Animals injected with any of three different *moz* MOs display dose-dependent homeotic phenotypes seen in *moz* mutants (Fig. 2C,F,I; Table 2), strongly supporting our conclusion that reduction of *moz* function causes the *b719* and *b999* homeotic phenotypes.

Injection of lower doses of each morpholino, as well as analyses of the slightly variable *b719* and hypomorphic *b999* phenotypes (Table 2), show that the several homeotic phenotypes described above are separable, and that homeosis is not an all-or-nothing phenomenon. Some mutant animals display shape changes of the dorsal hyoid cartilage (the HM cartilage) without having deletions of HM (Table 2), showing *moz* controls at least two processes, positioning and shaping, of dorsal second arch cartilage formation. Likewise, some mutant animals display homeotic shape changes of the ventral hyoid cartilage without displaying the inversion (Table 2), similarly arguing that these two processes are separable. Interestingly, shape changes are more frequently seen than fusions, regardless of MO or dose (Table 2). The dorsal deletion of the hyomandibular portion of the hyosymplectic was the least penetrant for both mutant alleles and with both doses of all three MOs (Table 2). Thus, sensitivity to reduction of *moz* function ranges from high for shape changes to intermediate for fusions to low for dorsal deletions.

moz is required for most Hox group 1-4 expression domains

As anterior transformation of arch two to one resembles the mouse *Hoxa2* and zebrafish *hoxa2b*;*hoxb2a* loss-of-function phenotypes (Gendron-Maguire et al., 1993; Rijli et al., 1993; Hunter and Prince, 2002) (C. T. Miller, PhD Thesis, University of Oregon, 2001), we asked if *moz* functions upstream of *hox2* genes. Although zebrafish have at least seven Hox clusters, only two *hox2* genes are retained, *hoxa2b* and *hoxb2a* (Amores et al., 1998). Expression of both *hoxa2b* and *hoxb2a* is broadly and severely downregulated in the *moz* mutant second arch primordia by 33 hpf (Fig. 3A-D, see below). Like the second pharyngeal arch expression and despite the separable regulation of pharyngeal arch and CNS Hox gene expression domains (Prince and Lumsden, 1994; Maconochie et al., 1999), hindbrain expression of *hoxa2b* is also severely reduced in *moz* mutants at 33 hpf (Fig. 3E,F). All rhombomeres that express *hoxa2b* (rhombomeres 2-5 or r2-r5) appear to do so at a lower level in *moz* mutants, although r2 appears to be the most strongly affected. Expression of *hoxa2b* is strikingly reduced

in medial r2 and lateral r4 (Fig. 3E,F). To determine if *hoxa2b* expression was simply delayed in *moz* mutants, we assayed a later time point, 48 hpf. Even with overdeveloped in situ hybridization and similar to expression at 33 hpf, arch expression of *hoxa2b* is undetectable (Fig. 3G,H), and hindbrain expression is still drastically reduced (data not shown).

To determine if *moz* is required for the initiation of expression of the Hox genes it regulates, we examined *hoxa2b* expression at 11 hpf, soon after it initiates embryonic expression (Prince et al., 1998). Initiation of *hoxa2b* expression in the hindbrain in *moz* mutants appears unaffected (Fig. 3I,J). However, initiation of *hoxa2b* in second arch CNC around 12-14 somites occurs but is substantially reduced in *moz* mutants (data not shown). Thus, *moz* regulates *hoxa2b* expression in distinct manners in the hindbrain and CNC.

We next asked if *moz* is required for expression of other Hox genes. *hoxa1a* expression is normally not present in a typical Hox domain spanning one or multiple segments but instead is in clusters of cells in the ventral forebrain and midbrain and in scattered cells in the anterior hindbrain (McClintock et al., 2001; McClintock et al., 2003). In contrast to the *moz* requirement for later expression of *hoxa2b* and *hoxb2a*, *hoxa1a* expression is not appreciably affected in *moz* mutants (Fig. 3K,L).

For the *hoxba* cluster, expression of group 1-4 genes are affected in a graded fashion in *moz* mutants, with *hoxb1a* being the most severely affected and *hoxb4a* the most mildly affected. Severe Hox expression defects in *moz* mutants are also present in the embryonic hindbrain. At 36 hpf, the r4-restricted hindbrain expression of *hoxb1a* is nearly abolished in *moz* mutants (Fig. 3M,N). In addition to the missing second arch domain (see above), hindbrain expression of *hoxb2a* is reduced in *moz* mutants (Fig. 3O,P). *hoxb3a* expression is reduced in the hindbrain and in the third to fifth pharyngeal arch primordia in *moz* mutants (Fig. 3Q,R), perhaps contributing to the third arch homeotic phenotype presented above. Expression of *hoxb4a* is mildly reduced in both the hindbrain and pharyngeal arches four through six of *moz* mutants (Fig. 3S,T). Expression of the other *hox3-4* genes is similarly affected as their respective *hoxb3a* and *hoxb4a* paralogs (data not shown). Initiation of Hox genes *b1a-b4a*, like *hoxa2b*, appears unaffected in the hindbrain of *moz* mutants. Hence, similar to *trithorax* group (*trx*G) genes (Simon and Tamkun, 2002; Ernst et al., 2002), *moz* appears to be required for the maintenance, but not initiation, of expression of particular Hox genes in the hindbrain.

However, *hox5-6* gene expression appears unaffected in *moz* mutants (Fig. 3U,V; data not shown). Thus, *moz* expression, present throughout the embryonic head (see Fig. 1C-E), is specifically required for most *hox1-4* expression domains in the hindbrain and pharyngeal arches.

Inhibition of histone deacetylase activity partially rescues the *moz* mutant phenotype

Because human MOZ has been shown to have histone acetyltransferase (HAT) activity (Champagne et al., 2001), and because *trx*G factors that maintain Hox gene expression are associated with HAT activity (Petruk et al., 2001; Milne et al., 2002), we wondered whether the inability of *moz* mutants to maintain Hox gene expression was due to hypoacetylation. The histone deacetylase inhibitor trichostatin A (TSA) has been
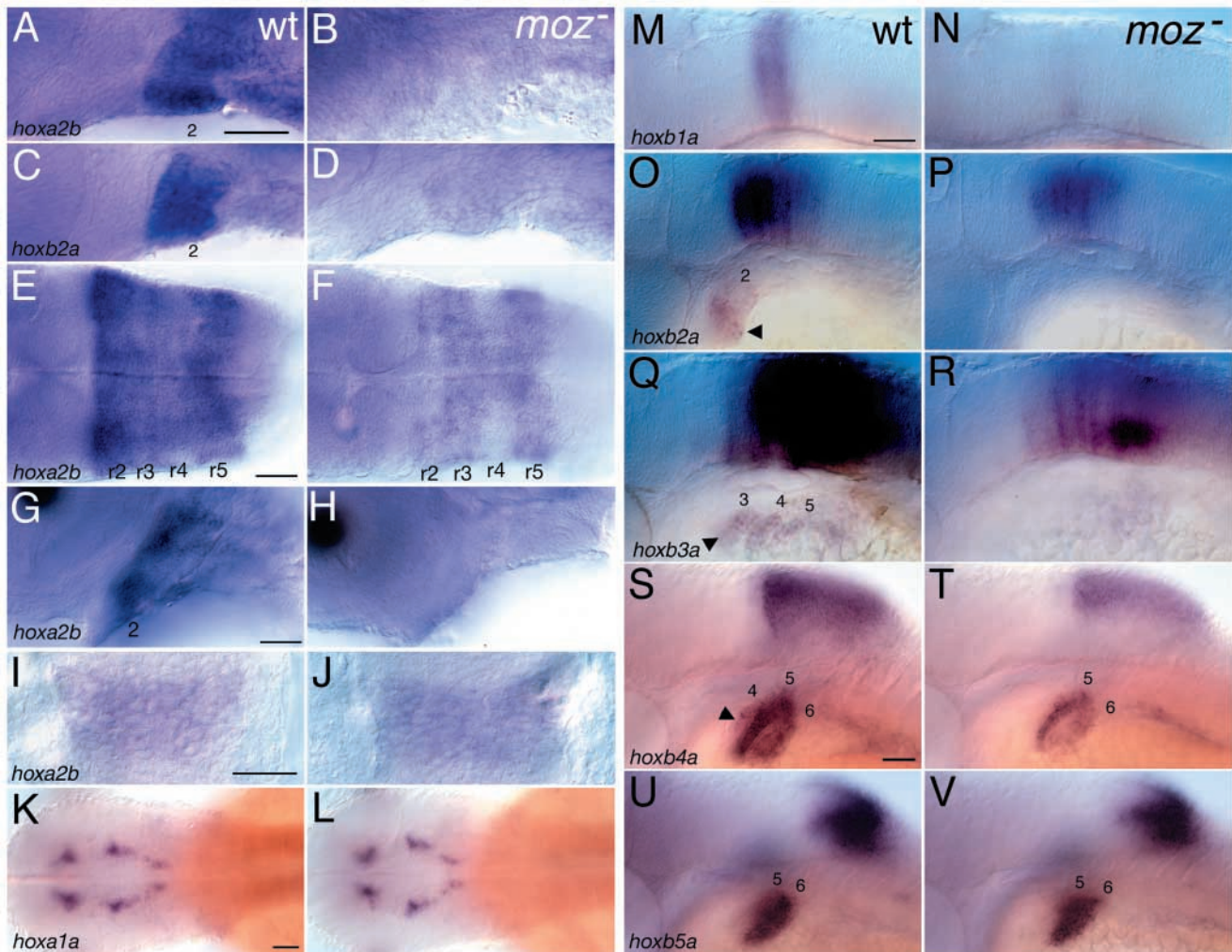
Fig. 3. *moz* is required for most *hox1-4* expression domains. Lateral (A-D,G-H,M-V) and dorsal (E-F,I-L) views of Hox expression in wild type (A,C,E,G,I,K,M,O,Q,S,U) and *moz* mutants (B,D,F,H,J,L,N,P,R,T,V) at 33 hpf (A-F), 11 hpf (I,J) and 48 hpf (G,H,K-V). (A,B) *hoxa2b* expression, which is present in arches two and three of wild type (A), is undetectable in these arches in *moz* mutants (B). (C,D) *hoxb2a* expression normally present in the second arch (C), is barely detectable in the *moz* mutant second arch (D). (E,F) *hoxa2b* expression in the hindbrain is reduced in *moz* mutants (G,H) *hoxa2b* expression in second arch CNC is severely reduced (I,J) Initiation of *hoxa2b* expression at 11 hpf occurs normally in *moz* mutants. (K,L) *hoxa1a* in the ventral forebrain and midbrain, and anterior hindbrain, is unaffected in *moz* mutants (M-V) Graded affect on *hoxb1a-b5a* gene expression in *moz* mutants. (M,N) *hoxb1a* expression in r4 is largely abolished in *moz* mutants. (O,P) *hoxb2a* expression in r3-5 is downregulated in *moz* mutants, and second arch expression (arrow) is now undetectable. (Q,R) *hoxb3a* expression in the caudal hindbrain is reduced, and pharyngeal arch expression in arches 3-5 (arrow) is undetectable. (S,T) *hoxb4a* expression is mildly reduced in the posterior hindbrain and pharyngeal arches 4-6 (arrow). (U,V) *hoxb5a* expression appears unaffected in *moz* mutants. Scale bars: 50 μm.

shown to rescue defects caused by *trx*G mutations in *Drosophila* (Sollars et al., 2003) and human cells (Milne et al., 2002). We therefore asked whether TSA treatment could rescue the *moz* mutant phenotype. *moz* mutant embryos that are incubated in 0.1 M TSA starting at about 15 hpf show striking rescue of arch cartilage homeosis (Table 3; Fig. 4A-D) and rescue of Hox gene expression (Fig. 4E-H).

TSA-treatment partially rescues *hoxa2b* expression in the hindbrain and second arch CNC of *moz* mutants (*n*=12/12) compared with DMSO-treated *moz* mutant controls (*n*=6/6; Fig. 4E-H). TSA-treated *moz* mutants (*n*=5/5) have increased, but not wild-type levels, of r4 expression of *hoxb1a* compared with DMSO-treated *moz* mutant controls (*n*=8/8) (not shown). TSA-treated *moz* mutants have weakly rescued expression of

hoxb2a in hyoid CNC (*n*=6/7) compared with DMSO-treated *moz* mutant controls (*n*=5/5, data not shown). Therefore, even though neither of our *moz* mutant alleles directly affect the Moz HAT domain, these results suggest that the *moz* homeotic phenotype is at least partially dependent on the function of Moz HAT activity.

moz mutants display late hindbrain neuronal phenotypes

Given the broad expression defects of group 1-4 Hox genes, we analyzed hindbrain neuronal development in *moz* mutants. Facial motoneurons differentiate in r4 and begin to migrate posteriorly towards r5-6 around 15 hpf (Chandrasekhar et al., 1997; Maves et al., 2002). At 48 hpf, some mutants display

Table 3. Histone deacetylase inhibitor trichostatin A (TSA) rescues *moz* mutant homeosis and *hox* gene expression defects

Treatment	Genotype and treatment			
	b719+/b719+ +DMSO	b719–/b719– +DMSO	b719+/b719+ +TSA	b719–/b719– +TSA
n	31	26	24	39
% with phenotype (*n*)				
Dorsal deletion	0 (0.0)	69 (18.0)	0 (0.0)	22 (8.5)
Dorsal shape change	0 (0.0)	100 (26.0)	46 (11.0)	76 (29.5)
Ventral inversion	0 (0.0)	95 (25.0)	0 (0.0)	8 (3.0)
Ventral shape change	0 (0.0)	52 (13.5)	0 (0.0)	6 (2.5)
Ventral fusion	0 (0.0)	60 (15.5)	0 (0.0)	0 (0.0)
Dorsal fusion	0 (0.0)	39 (10.0)	0 (0.0)	0 (0.0)

All animals were PCR-genotyped. See Table 2 legend for scoring method and explanation of phenotypes and abbreviations. The HS disorganization in TSA-treated embryos, while disorganized relative to the untreated wild-type pattern, lacked shape changes characteristic of *moz* mutants.

mispositioned facial motoneurons (Fig. 5A,B), resembling *hoxb1* loss-of-function phenotypes seen in zebrafish and mice (McClintock et al., 2002; Studer et al., 1996; Goddard et al., 1996; Gavalas et al., 2003). In contrast to *Mll*/Trithorax mutant mice, which also fail to maintain Hox expression (Yu et al., 1998), cranial ganglia appear to innervate each pharyngeal arch (Fig. 5C,D). The early reticulospinal neurons, some of which are born by 10 hpf (Mendelson, 1986) and show anterior transformations upon reduced function of *hoxb1* (McClintock et al., 2002), display no detectable alterations in *moz* mutants (data not shown). Thus, early segmentation and neuronal specification of the *moz* mutant hindbrain occurs relatively normally, while later hindbrain phenotypes in *moz* mutants are consistent with a defect in maintenance, but not initiation, of Hox gene expression.

Late patterning defects in *moz* mutant arch mesoderm

Segmental identity in the vertebrate head periphery involves complex crosstalk between CNC and head mesoderm. In the mouse, Hox gene expression in CNC requires unknown factors emanating from cranial mesoderm (Trainor and Krumlauf, 2000). Conversely, in the chick, transplanting (presumably *Hoxa2*-negative) first arch CNC into the second arch results in second arch muscles non-autonomously adopting a first arch pattern of beak muscles (Noden, 1983a; Trainor et al., 2002). In zebrafish, mosaic analyses have revealed that CNC patterns arch mesoderm (Schilling et al., 1996b; Knight et al., 2003). Additionally, zebrafish injected with hox2-MOs and *Hoxa2* mutant mice display altered head musculature (Rijli et al., 1993; Barrow and Capecchi, 1999; Hunter and Prince, 2002). Thus, we expected head musculature to be affected in *moz* mutants but wondered at what stage segmental identity defects in the head mesoderm occur.

Pharyngeal arch muscles are derived from paraxial mesoderm, which initially occupies central locations (arch 'cores') in the pharyngeal arch, ensheathed by postmigratory CNC (reviewed by Kimmel et al., 2001b). Each arch mesodermal core subdivides into a discrete pattern of identified myogenic cores. The first and second arches display different sequences of mesodermal core subdivision. Although at intermediate stages in fish the first arch contains three myogenic cores [constrictor dorsalis (CD), adductor mandibulae (AM) and intermandibularis (IM)], the second arch
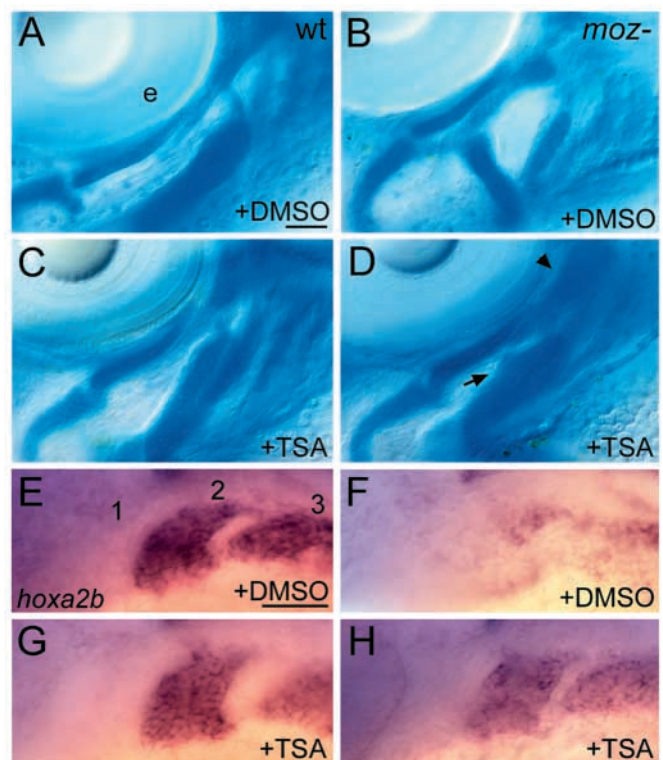

Fig. 4. Rescue of skeletal homeosis and *hoxa2b* expression in *moz* mutants by the histone deacetylase inhibitor Trichostatin A (TSA). (A-D) Ventrolateral views of 4-day-old wild type (A,C) and *moz* mutant (B,D) larvae treated with DMSO (A,B) or TSA (C,D) stained with Alcian Green. TSA rescues many aspects of the skeletal phenotype, including deletion of the HM cartilage (arrowhead) and fusion and inversion of the ventral second arch cartilage (arrow; see Table 3). (E-H) Lateral views of *hoxa2b* expression at 33 hpf in wild type (E,G) and *moz* mutants (F,H) treated with DMSO (E,F) or TSA (G,H). TSA treatment rescues *hoxa2b* expression in *moz* mutants. e, eye. Scale bars: 50 µm.

contains only two [constrictor hyoideus dorsalis and ventralis (CHD and CHV)]. These myogenic cores subsequently subdivide into primordia for individual muscles (Edgeworth, 1935) (reviewed by Kimmel et al., 2001b). This early difference in the wild-type arch one and two intermediate
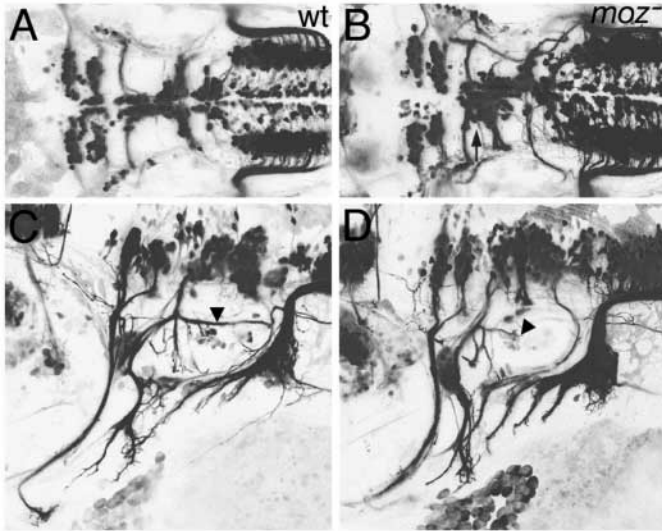
Fig. 5. Neuronal patterning defects in *moz* mutants. (A-D) Cranial motoneurons labeled by Islet1:GFP (Higashijima et al., 2000) at 48 hpf in wild type (A,C) and *moz* mutants (B,D). (A,B) Most *moz* mutants (52%, 11 of 21) show defects in cell body positioning of facial motoneurons (arrow). (C,D) Cranial nerves innervate each pharyngeal arch in *moz* mutants. The VIIIth nerve octavolateralis efferent (arrowheads in C,D) is variably mispatterned in *moz* mutants, resembling the phenotype seen in hoxb1a-MO injected larvae (McClintock et al., 2002).

myogenic core pattern precludes assigning segmental homology to subsequently-forming dorsal and intermediate muscles. However, this intermediate pattern serves as a segmental character distinguishing the first two arches. Thus, we wondered whether this aspect of segmental identity was transformed in *moz* mutants.

eng2 expression marks the dorsal first arch myogenic condensation, constrictor dorsalis (Hatta et al., 1990; Ekker et al., 1992) (reviewed by Kimmel et al., 2001b). Expression of *eng2* in *moz* mutants at 28 hpf is not seen homeotically duplicated in the second arch (Fig. 6A,B). *myod* expression marks all pharyngeal arch myogenic condensations (Schilling and Kimmel, 1997). We examined *myod* expression in *moz* mutants at 44 hpf, a stage soon after *myod* expression labels the first and second arch myogenic condensations (Fig. 6C,D). The arrangement of *myod*-expressing cores in *moz* mutants at this stage appears grossly indistinguishable from the wild-type pattern (Fig. 6C,D). Slightly later in development at 54 hpf, subtle defects are observed in *moz* mutant *myod*-expressing myogenic condensations. Ectopic patches of *myod* expression are seen in the intermediate second arch of *moz* mutants (Fig. 6E,F).

Despite the lack of dramatic early muscle phenotypes, the larval musculature at 4 days is radically transformed in *moz* mutants (Fig. 6G,H). In wild types, a large jaw-closing adductor mandibulae muscle connects the dorsal and ventral cartilages in the first arch, whereas no prominent muscles connect the dorsal and ventral cartilages in the second arch (Fig. 6G). In *moz* mutants, the first arch muscle pattern appears unaffected, except for late subdivision and patterning of CD, which normally inserts upon the HM cartilage. In most (61%, 14/23) *moz* mutants, a muscle of variable size in the second arch connects
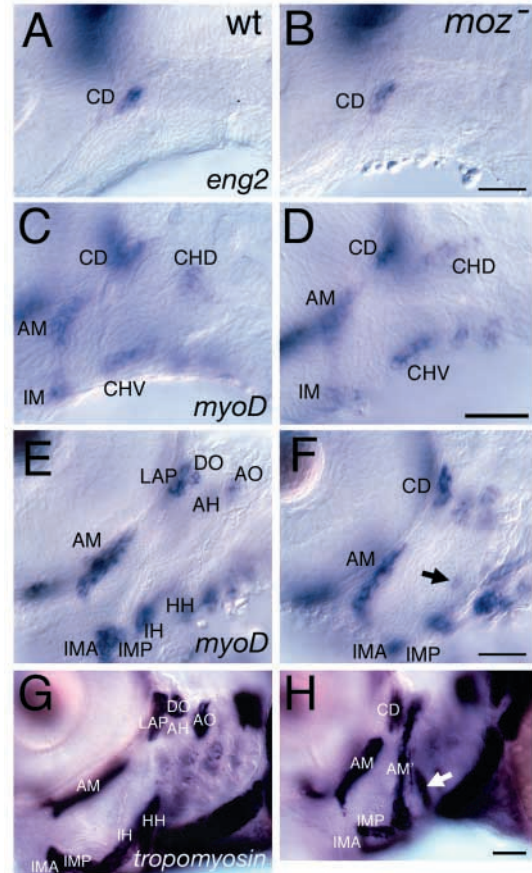

Fig. 6. Late, but not early, muscle defects in *moz* mutants. (A,B) *eng2* expression in wild types marks the dorsal first arch myogenic core, CD, which is not homeotically duplicated in *moz* mutants. (C-F) *myod* expression in wild type (C,E) and *moz* mutants (D,F) at 44 hpf (C,D) and 54 hpf (E,F). (C,D) *myod* expression marks three first arch and two second arch myogenic cores. The *moz* mutant second arch pattern at this stage appears normal. (E,F) By 54 hpf *moz* mutant musculature looks aberrant. A small ectopic patch of *myod* is present in the intermediate second arch (arrow in F). (G,H) Lateral views of α-tropomyosin expression in wild type (G) and *moz* mutant (H). In wild types (G), a large jaw closing muscle (am) connects the upper and lower jaw. *moz* mutants appear to have an ectopic jaw closer muscle (am′) in their second arch (H). This muscle appears continuous with what we interpret to be the remnants of the dorsal (AH and AO) and ventral muscles (IH and HH) and the first arch dorsal muscles (LAP and DO) appear to not have segregated as they have in wild types. An enlarged third arch muscle is present (white arrow in H) in *moz* mutants. AH, adductor hyomandibulae; AM, adductor mandibulae; AO, adductor operculi; DO, dilator operculi; HH, hyohyal; IH, interhyal; IMA, intermandibularis anterior; IMP, intermandibularis posterior; LAP, levator arcus palatini. Scale bars: 50 μm.

the dorsal and ventral cartilages (Fig. 6H). These late muscle phenotypes in *moz* mutants resemble a slightly stronger version of those reported for hox2-MO injected zebrafish (Hunter and Prince, 2002). In *moz* mutants in which a muscle did not connect the dorsal and ventral hyoid cartilages, hyoid musculature was variably disorganized. Without specific markers for individual hyoid muscles, we were unable to assign identity to these. The third arch ventral muscle (transversus ventralis) (Schilling and Kimmel, 1997) was slightly enlarged

in *moz* mutants, suggesting, like the cartilage phenotype, a mild anterior homeotic transformation. Together these results indicate that *moz* mutants display late, but not early, anterior homeotic transformations of second and third arch musculature.

Defects in pharyngeal epithelia are not detected in *moz* mutants

Pharyngeal endoderm is required for many aspects of CNC patterning (Piotrowski and Nüsslein-Volhard, 2000; Piotrowski et al., 2003; Couly et al., 2002) and chondrification of CNC requires contact with pharyngeal endoderm (Epperlein, 1974). Given that the hyomandibular (HM) region of the dorsal second arch cartilage almost never chondrifies in *moz* mutants (Table 2), we wondered whether missing, mispositioned or mis-specified pharyngeal pouches contribute to the *moz* mutant phenotype.

We directly assayed developing pharyngeal pouch morphology and specification by following the expression of the FGF target gene *pea3* (Roehl and Nüsslein-Volhard, 2001) at 24, 34 and 54 hpf. Each pharyngeal pouch, which separates the arch primordia, consists of an epithelial bilayer with an AP polarity: expression of *pea3* and the secreted ligand *edn1* are both expressed in posterior, but not anterior, pharyngeal endodermal epithelia (Fig. 7A,B) (Miller et al., 2000). The first pharyngeal pouch, which abuts dorsal second arch CNC, is present in *moz* mutants and appears similarly patterned as its wild-type counterpart at all three stages examined (Fig. 7A,B; data not shown). The same was true for more posterior pharyngeal pouches (Fig. 7A,B; data not shown). We wondered if the mirror-image duplication of the first arch pattern in the *moz* mutant second arch could be due to defects or possibly even reversals in pharyngeal pouch polarity. However, expression of *pea3* (Fig. 7A,B) and *edn1* (data not shown) in *moz* mutants revealed no defects in pouch polarity.

Surrounding ectodermal epithelia also contribute to CNC patterning (Tyler and Hall, 1977). *shh* is specifically expressed in a thin stripe of second arch surface ectoderm at the posterior margin of the second arch resembling an identified *shh* expression domain in chicks and mice (posterior ectodermal margin or PEM of the second arch) (Wall and Hogan, 1999). Given the second arch specificity of this pattern and the defect in second arch identity in *moz* mutants, we wondered whether *moz* mutants might lack this expression domain of *shh*. Instead, expression of *shh* in *moz* mutants is still present in the PEM of the second arch, although expression is perhaps slightly reduced ventrally (Fig. 7C,D). Thus, this epithelial aspect of hyoid segmental identity is retained in *moz* mutants.

Between the inverted ectopic jaw and the enlarged third arch in *moz* mutants, large bilateral openings in the pharynx resemble ectopic mouths (see Fig. 2B). To determine if gene expression data support this interpretation, we examined expression of a stomadeal marker, *pitx2c* (Essner et al., 2000; Schweickert et al., 2001), in *moz* mutants. *pitx2c* expression in wild-type embryos at 54 hpf strongly labels the mouth, presumably the ectodermal derivatives of the stomodeum (Fig. 7E,F). Expression of *pitx2c* in *moz* mutants was not detected ectopically in these enlarged pharyngeal openings, providing no evidence for stomadeal identity.

In chicks, the thymus forms largely from the third and fourth endodermal pharyngeal pouches, which attract blood-borne lymphocyte precursors (LeDouarin and Jotereau, 1975). In mice, *hox3* genes regulate thymus formation (Manley and
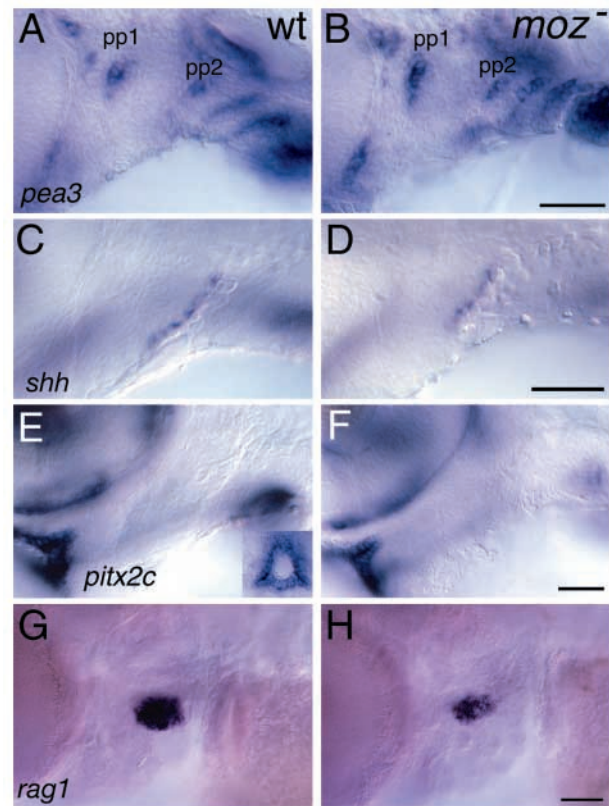

Fig. 7. Early patterning of arch epithelial tissues appears unaffected in *moz* mutants. Lateral views of wild-type (A,C,E,G) and *moz* mutant (B,D,F,H) embryos at 34 hpf (A,B), 41 hpf (C,D), 54 hpf (E,F) and 4 days (G,H). (A,B) *pea3* expression marks posterior pharyngeal endodermal epithelia. No inversion of this pattern is seen in *moz* mutant pouches. First and second pharyngeal pouches are outlined. (C,D) *sonic hedgehog* (*shh*) expression marks the posterior ectodermal margin (PEM) of the second arch, a thin line of cells marking the posterior edge of the forming opercular flap. PEM expression persists in *moz* mutants. (E,F) *pitx2c* expression strongly labels the mouth in wild type and *moz* mutant. No ectopic *pitx2c* expression is seen in the mouth-like openings between the second and third arch in *moz* mutants. (G,H) *rag1* expression labels a reduced but present thymus in *moz* mutants. pp1, pharyngeal pouch 1; pp2, pharyngeal pouch 2. Scale bars: 50 μm.

Capecchi, 1995; Manley and Capecchi, 1998). In zebrafish, *rag1* expression in lymphocytes marks the early thymus (Willett et al., 1997). In *pbx4*(*lzr*) mutants, which have reduced *hox3* expression, the thymus fails to form as assayed by *rag1* expression (Popperl et al., 2000). Thus, we similarly asked whether *moz* mutants form a thymus by examining *rag1* expression at 4 days. *rag1* expression in the thymus is present in *moz* mutants, although reduced (Fig. 7G,H). Taken together, these results reveal relatively minor defects in arch epithelial tissues in *moz* mutants and are consistent with the idea that many aspects of the arch environment are set up independent of the CNC (Veitch et al., 1999; Gavalas et al., 2001).

Early CNC generation appears normal in *moz* mutants but mispositioned and misshapen condensations form

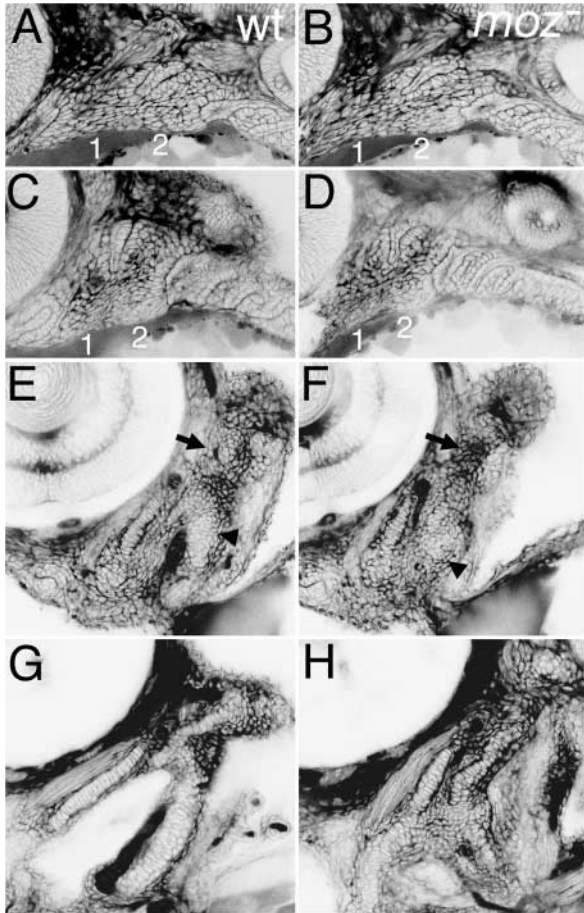Finding evidence suggesting that early patterning of non-CNC

Fig. 8. Hyoid CNC is generated in *moz* mutants but forms mispositioned and misshapen condensations. Confocal micrographs of lateral views of the anterior pharyngeal arches in live wild-type (A,C,E,G) and *moz* mutant (B,D,F,H) embryos (A-F) and larvae (G-H) stained with the vital fluorescent dye BODIPY-ceramide at 28 hpf, 34 hpf, 48 hpf and 3.5 day stages. Images have been inverted; the dye fills interstitial spaces, so the inverted images show cells labeled in white and interstitial space in black. (A,B) Early CNC appears morphologically indistinguishable from wild type in *moz* mutants. Both first and second arches are filled with a cylinder of postmigratory CNC (Miller et al., 2000; Kimmel et al., 2001b), with no obvious defect in hyoid or branchial CNC in mutants. Other arch tissues also fail to show obvious morphological defects (C,D). At a slightly later stage the second pharyngeal arch in *moz* mutants appears slightly hypoplastic (D), but is still filled with CNC. (E,F) A day later, condensations have formed in the wild type (E), including in the second arch a dorsal hyomandibular condensation (arrow, compare with Fig. 2D) and a ventral ceratohyal condensation (arrowhead). In *moz* mutants, no dorsal second arch hyomandibular condensation is seen and cells appear as lose mesenchyme in this region (arrow in F). A dorsal mutant condensation does form, in the position of the wild-type symplectic condensation. The ventral mutant condensation is mispositioned anteriorly (arrowhead), and is abutting the first arch ventral condensation. The condensation pattern (E,F) largely prefigures the resultant larval cartilage pattern (G,H; compare with Fig. 2D,E). This figure shows two time points of four different animals: A and C are the same animal, as are B and D, E and G, and F and H. Arches are numbered in A-D.

arch tissues is normal in *moz* mutants, we next analyzed the CNC. In mice, Hox genes not only control segmental identity, but also control the generation of CNC (Gavalas et al., 2001). To determine whether the broad Hox expression defects result in a defect in CNC generation, we examined early pharyngeal arch primordia in living embryos with the fluorescent dye BODIPY ceramide. This vital labeling offers nice histological resolution of all major differentiated cell types (Kimmel et al., 2001b; Yan et al., 2002). Examining arch primordia in labeled embryos from clutches of *moz* mutants revealed mutants to be morphologically indistinguishable from their wild-type siblings around 28 hpf when postmigratory CNC has populated the arch and surrounded the mesodermal cores. No deficit in hyoid CNC was apparent (Fig. 8A,B). Consistent with this, expression of the broadly expressed CNC marker *dlx2* at 28 hpf appears unaffected in *moz* mutants (data not shown). Slightly later, around a 34 hpf stage, the *moz* mutant hyoid arch appears slightly hypoplastic (Fig8C,D), although gross arch morphology appears relatively normal. These same optical sections confirm our in situ results that no gross changes are apparent in the early pharyngeal pouches in *moz* mutants (see above).

In *jellyfish/sox9a* mutant zebrafish, which lack nearly all cartilage, condensations form but subsequently fail to differentiate (Yan et al., 2002). We wondered if the *moz* mutant hyomandibular cartilage, which almost never forms (Fig. 2A,B; Table 2), forms a condensation but fails to differentiate. Examining BODIPY-labeled animals at later timepoints

revealed the condensation pattern in *moz* mutants to be extremely aberrant around 48 hpf and predictive of disruption of the larval cartilage pattern at 3.5 days (Fig. 8E-H). In the *moz* mutant dorsal second arch, no trace of an HM condensation is seen. Instead, the dorsal second arch condensation is shifted ventrally (Fig. 8E,F). Likewise, the lateral end of the ventral second arch condensation is displaced anteriorly, abutting the lateral end of the lower jaw cartilage condensation (Fig. 8E-H). Thus, the positioning and shaping processes that *moz* controls in the larval cartilage pattern begin prior to condensation formation.

moz and *hox2* genes repress early second arch expression of *bapx1*, which is required for aspects of *moz*-mediated homeosis

Reduced *hox2* expression can at least in part account for the anterior transformation homeotic skeletal and muscular phenotypes observed in the second arch of *moz* mutants. To investigate the molecular consequences of *hox2* downregulation in the early second arch primordium, we analyzed embryonic expression of a known *hox2* target gene, *bapx1* (Pasqualetti et al., 2000), in *moz* mutants and in embryos injected with morpholinos to reduce function of *hoxa2b* and *hoxb2a*.

In embryos and larvae, *bapx1* is expressed in a patch of intermediate first arch, but not second arch, mesenchyme (Fig. 9A,D) (Miller et al., 2003). In *moz* mutants at 33 hpf, first arch *bapx1* expression is present while an ectopic *bapx1* domain is seen in the second arch (Fig. 9B,E), providing molecular confirmation of an anterior transformation in second arch CNC of *moz* mutants. Ectopic second arch *bapx1* expression is also observed in embryos injected with *hoxa2b* and *hoxb2a* morpholinos (95%, 37/39; Fig. 9C), demonstrating that *hox2*
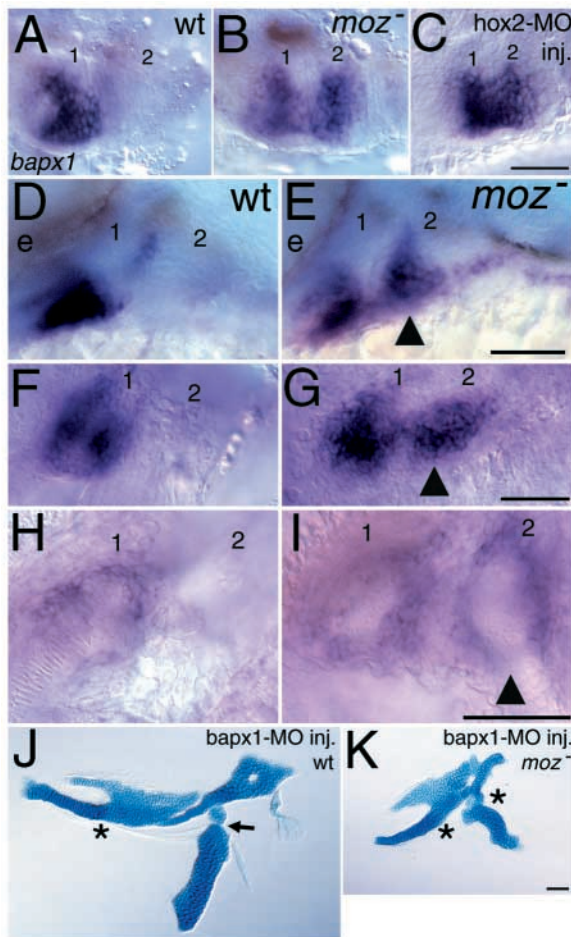
Fig. 9. Stable ectopic expression of *bapx1* in the *moz* mutant second arch. Ventral (A-C,F-I) and lateral (D,E) views of *bapx1* expression in whole-mount wild-type (A,D,F,H), *moz* mutant (B,E,G,I) and *hoxa2b + hoxb2a*-MO co-injected animals (C) at 33 hpf (A-E), 54 hpf (F,G) and 4 days (H,I). (A-E) *bapx1* expression, which is normally restricted to a patch of first arch mesenchyme (A,D), is ectopically expressed (arrowhead in E) in the second arch of *moz* mutants (B,E) and *hoxa2b+hoxb2a*-MO co-injected animals (C). (F-I) Ectopic *bapx1* expression (arrowheads) is maintained in second arch mesenchyme of *moz* mutants. (J,K) Reduction of *bapx1* function in wild type (J) and *moz* mutant (K). Reducing *bapx1* function in wild type causes specific loss of the jaw joint (asterisk in J), while reducing function of *bapx1* in *moz* mutants causes loss of both first and second arch joints (asterisks in K). Reduction of *bapx1* function in *moz* mutants also can rescue the ventral arch one and two fusions. The first two pharyngeal arches are numbered. e, eye. Scale bars: 50 μm.

dysfunction is sufficient to result in these homeotic molecular changes. Ectopic *bapx1* expression is present in *moz* mutants and hox2-MO injected animals when *bapx1* expression first initiates arch expression, around 30 hpf (data not shown). This molecular homeosis is stable, as *bapx1* expression is maintained in the second arch at 54 hpf (Fig. 9F,G) and 4 days (Fig. 9H,I).

We next asked if this ectopic *bapx1* expression domain is functional in *moz* mutants. Reducing *bapx1* function in a wild-type background specifically eliminates the jaw joint and does not affect the second arch joint (Miller et al., 2003) (Fig. 9J). Reducing *bapx1* function in a *moz* mutant background now

Table 4. *bapx1* is required for both arch one and arch two joints in *moz* mutants

		% lacking joints	
	Genotype	Arch 1	Arch 2
Control	Wild type	0 (0/120)	0 (0/120)
	moz-	0 (0/42)	4 (1.5/42)
bapx1-MO	Wild type	89 (74/83)	0 (0/83)
	moz-	91 (24.5/27)	70 (19/27)*

*Significantly higher in *moz* mutants (*P*<0.001 by chi-square).
Control uninjected animals and bapx1-MO injected animals were PCR genotyped, then assayed for skeletal morphology in cleared Alcian Green stained whole-mount preparations.

results in loss of joints in both arch one and two (Fig. 9K; Table 4). Thus, the *moz* mutant second arch requires *bapx1* function for formation of the dorsal/ventral joint, providing functional genetic evidence that the *moz* mutant second arch phenotype is homeotic.

moz and *hox2* genes regulate the mediolateral pattern of *goosecoid* expression in the second arch

We extended our analyses of early CNC patterning in *moz* mutants by studying expression of a second known *hox2* target gene, *goosecoid* (*gsc*) (Grammatopoulos et al., 2000; Pasqualetti et al., 2000; Hunter and Prince, 2002). Misexpression of *hoxa2* in the chick and *Xenopus* induces *gsc* expression (Grammatopoulos et al., 2000; Pasqualetti et al., 2000). In zebrafish, *hoxa2b* and *hoxb2a* were reported to positively regulate early second arch *gsc* expression, although only lateral views were reported (Hunter and Prince, 2002).

Viewing early embryonic *gsc* expression from a ventral aspect reveals *gsc* expression to consist of a thin medial crescent in the ventral first arch and a broad lateral crescent in the ventral second arch (Fig. 10A). Examination of *gsc* expression in *moz* mutants from this ventral aspect reveals a startling patterning change. In *moz* mutants, ventral second arch expression of *gsc* appears as a thin medial crescent, mirroring the first arch pattern (Fig. 10B). Like the *bapx1* expression change, this shifting of *gsc* expression is also observed in embryos injected with *hoxa2b* and *hoxb2a* morpholinos (92%, 23/25; Fig. 10C), demonstrating that *hox2* dysfunction is also sufficient to result in this homeotic molecular change of *gsc* expression. At 41 hpf, dorsal arch two expression of *gsc* is reduced (Fig. 10D,F). However, lateral views do not reveal maintenance of the patterning change that ventral views do: the shifting of lateral *gsc* expression to the medial second arch (Fig. 10E,G). The pattern at 41 hpf is slightly different than the 33 hpf pattern (Fig. 10H), suggesting *gsc* expression is either dynamic, and/or that movements of *gsc*-expressing cells occur. Together our results suggest *moz* not only controls maintenance of an early pattern, but also specification of subsequent dynamic changes in patterning in the second arch CNC well before differentiation begins.

Discussion

An essential embryonic role for the oncogene *moz*

In humans, translocation breakpoints within *MOZ* result in leukemia (Borrow et al., 1996; Aguiar et al., 1997; Carapeti et
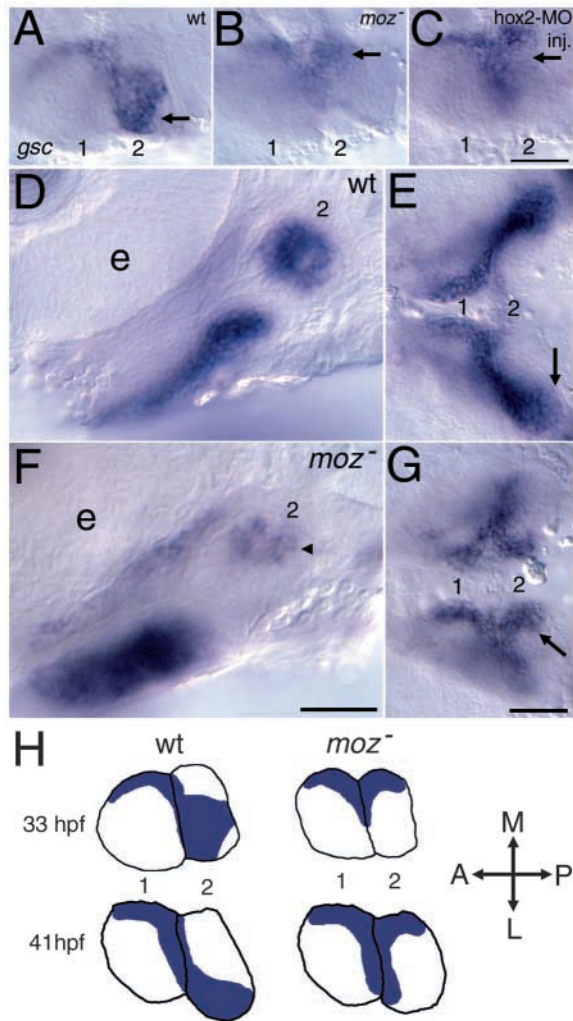
Fig. 10. Mirror-image duplication of *gsc* expression in the *moz* mutant second arch. Ventral (A-C,E,G) and lateral (D,F) views of *gsc* expression in whole-mount wild-type (A,D,E), *moz* mutants (B,F,G) and *hoxa2b+hoxb2a*-MO co-injected animals (C) at 33 hpf (A-C) and 41 hpf (D-G). In *moz* mutants and *hoxa2b+hoxb2a*-MO co-injected animals, second arch expression shift medially (arrows in B and C), mirroring the wild-type first arch pattern. (D-G) At 41 hpf in *moz* mutants, dorsal second arch *gsc* expression is reduced (arrowhead in F) and ventral expression is still inverted (arrows in E,G). (H) Schematic of expression domains visible in (A,B,E,G). In *moz* mutants, lateral second arch *gsc* expression is missing, and instead the second arch pattern resembles a mirror-image duplication of the first arch pattern, with a thin medial crescent of expression in the anterior medial arch. Relevant pharyngeal arches are numbered. e, eye. Scale bars: 50 μm.

al., 1998; Carapeti et al., 1999; Liang et al., 1998; Chaffanet et al., 2000; Kitabayashi et al., 2001b). Other regulators of Hox genes, including the mammalian ortholog of *Drosophila trithorax*, *MLL* also mutate to cause human leukemia (reviewed by Ernst, 2002). As Hox genes are normally expressed in hematopoietic lineages, it has been proposed that deregulated Hox expression contributes to many forms of leukemia (reviewed by Look, 1997). In support of this, deregulated Hox expression is associated with leukemia, and misexpression of individual Hox genes is sufficient to induce leukemia in mice

(Armstrong et al., 2002; Yeoh et al., 2002; Rozovskaia, 2001; Kroon et al., 1998; Magli et al., 1997). Our findings that zebrafish *moz* regulates Hox gene expression raises the question of whether deregulated Hox gene expression underlies *MOZ*-mediated leukemias.

Although no other in vivo functional data have been reported for *moz* in other vertebrates, biochemistry on human MOZ has revealed multiple functional domains. These domains include a founding HAT domain of the MYST family, an N-terminal transcriptional repression domain, and a C-terminal transactivation domain (Champagne et al., 2001; Kitabayashi et al., 2001a). MOZ additionally contains two C4HC3 zinc fingers and a C2HC nucleosome recognition motif (Borrow et al., 1996). This composite structure suggests MOZ can bind other proteins and chromatin, acetylate histones, and modulate transcription. Our *moz* alleles are predicted to truncate the C terminus, causing loss of a transcriptional activation (TA) domain, but leaving the HAT domain intact. However, the severely reduced *moz* mRNA levels detected by in situ hybridization in *moz^{b719}* mutants makes it likely that the overall activity of the remaining protein would be greatly reduced. This reduced expression of *moz* in *moz^{b719}* mutants suggests that *moz^{b719}* mutant transcripts are unstable or that *moz* directly or indirectly regulates its own transcription.

Both *moz* lesions we present are loss of function lesions, as mutant phenotypes are phenocopied by morpholino injections. However, we cannot rule out the possibility that both alleles and morpholino phenotypes are all hypomorphic until deletion alleles are found. Although we have no evidence of a fish-specific duplication of *moz*, vertebrates do have a closely related gene, *Morf* (monocytic leukemia zinc finger protein related factor; Myst4 – Mouse Genome Informatics), which is also mutated in human leukemias (Champagne et al., 1999; Panagopoulos et al., 2001). An embryonic function has been reported for *Morf* (named Querkopf) in mice (Thomas et al., 2000). An insertion in the 5′UTR of mouse MORF causes skull and forebrain defects, but hindbrain or homeotic pharyngeal arch defects were not reported (Thomas et al., 2000). Whether MORF and MOZ have overlapping functions is unknown.

Biochemical analyses of human MOZ have also revealed multiple MOZ-interacting partners. MOZ physically interacts with RUNX1 (AML1) and RUNX2 (AML3 or CBFA1) (Kitabayashi et al., 2001b; Pelletier et al., 2002). The RUNX2 interaction is particularly interesting, as this is the osteogenic gene shown in mice to be repressed by *Hoxa2* (Kanzler et al., 1998). Thus, in our analyses of segmental identity in the pharyngeal arches of *moz* mutants, we examined pharyngeal bones expecting to see ectopic bone formation. However, the hyoid bone pattern (Kimmel et al., 2003) was undetectable and duplicated mandibular bones were not seen in *moz* mutants (C.M., unpublished). Although we did not examine bone patterning in hox2-MO injected fish, one possibility is that MOZ functionally interacts with RUNX2 during pharyngeal development in zebrafish.

Whether mammalian MOZ regulates Hox gene expression, as we predict, awaits generation of *moz* mutant mice. The regulation of *Hoxa2* by the transcription factor AP2 is conserved from mammals to fish (Maconochie et al., 1999; Knight et al., 2003). However, no reduction in AP2 expression was observed in *moz* mutants at 28 hpf (C.M., unpublished results). Thus, the

regulation of *hox2* genes by *moz* appears to act through another mechanism, possibly by directly transactivating Hox genes.

moz regulates segmental identity of pharyngeal cartilages

Our results extend the understanding that Hox genes specify segmental identity in the vertebrate pharynx, as the transformed pharyngeal segments in *moz* mutants correlate with reduced Hox expression in pharyngeal arch primordia. A mirror-image duplicated jaw replaces the hyoid cartilages in *moz* mutants, resembling the phenotype seen in animals co-injected with *hoxa2b* and *hoxb2a* morpholinos (C. T. Miller, PhD Thesis, University of Oregon, 2001) (Hunter and Prince, 2002). However, the *moz* mutant transformation is more complete, as dorsal transformations are more severe and dorsal fusions more common than in hox2-MO injected animals. It is likely that morpholinos cause incomplete loss-of-function at later developmental timepoints when the injected morpholino is significantly diluted. Alternatively, *moz* might regulate other genes that are also expressed in hyoid CNC and contribute to segmental identity.

Despite this stronger phenotype, the homeotic transformation in the hyoid arch of *moz* mutants is still not complete in that the pterygoid process of the palatoquadrate (PTP) is not seen duplicated. Perhaps in *moz* mutants, as has been proposed for mouse *Hoxa2* mutants, only certain axial levels of CNC are transformed, i.e. perhaps PTP is derived from midbrain crest whose derivatives are not seen duplicated in the second arch of *Hoxa2* mutants (Köntges and Lumsden, 1996). de Beer (de Beer, 1937) proposed that PTP was a premandibular element.

The pharyngeal arches are more sensitive to partial reduction of *Hoxa2* function in the mouse (Ohnemus et al., 2001). The partial transformations observed in these hypomorphic mouse mutants led these authors to propose that homeosis was not an 'all-or-nothing' phenomenon, as the second arch did not act as a developmental unit as a whole. Our results, in which a hypomorphic allele and low-level injections of Moz-MOs also separate particular homeotic phenotypes from others, strongly support this conclusion.

Experiments in *Xenopus* with an inducible *Hoxa2* construct revealed that the time of *Hoxa2* overexpression affected the resultant phenotype: overexpressing *Hoxa2* early during CNC migration resulted in 'segmentation' phenotypes, where arch derivatives were fused, while overexpressing late in postmigratory CNC resulted in 'homeotic' phenotypes, where cartilage shapes were altered (Pasqualetti et al., 2000). As interarch fusions could also be interpreted as homeosis (i.e. loss of individual arch identity), this distinction is debatable. However, we note that the *moz* mutant phenotype contains more frequent shape changes ('homeotic') than fusions ('segmentation'), both dorsally and ventrally for both mutant alleles and for all three morpholinos at two different doses each. *pbx4*(*lzr*) mutants might display the converse phenotype, i.e. segmentation appears more affected than homeosis. Interarch fusions seen in *moz* mutants resemble the *pbx4*(*lzr*) mutant phenotype, although fusions are more severe in *pbx4*(*lzr*) mutants (Pöpperl et al., 2000). The more severe phenotype of *pbx4*(*lzr*) mutants might reflect differences in the set of affected target genes and/or temporal differences of target gene regulation (e.g. initiation versus maintenance).

moz mutants also present with mild anterior homeotic transformations of pharyngeal arches three and four (branchial or gill-bearing arches one and two). Arch three and four cartilages in *moz* mutants are slightly thicker, and typically contain an enlarged process on their lateral end, resembling the retroarticular process of Meckel's (the lower jaw) cartilage. Especially in the third arch of *moz* mutants at 5 days, an ectopic dorsal cartilage is also frequently seen. These transformations in the *moz* mutant anterior branchial arches are not seen in hox2-MO injected animals (Hunter and Prince, 2002). These phenotypes probably result from additional Hox genes (e.g. *Hox3* and *Hox4* genes) that *moz* regulates (see above). Once genetic alleles of these zebrafish Hox genes are isolated, their function in specifying pharyngeal segmental identity can be assessed.

This third arch cartilage phenotype in *moz* mutants somewhat resembles the phenotype of *valentino* (*val*) mutants (Moens et al., 1998) (reviewed by Kimmel et al., 2001a), which was interpreted to be an ectopic interhyal cartilage based on ectopic *hoxb2a* expression in the third arch of *val* mutants. As neither *hoxa2* nor *hoxb2* is expressed in the *moz* mutant third arch, we propose that the *moz* mutant third arch has adopted mandibular fate. We did not detect ectopic *bapx1* expression in third or fourth arch CNC of *moz* mutants. However, given the subtle nature of the skeletal change, the causative gene expression changes would probably be subtle as well.

Moz is required for Hox maintenance and behaves like a trithorax group factor

Consistent with the homeotic pharyngeal arch phenotype, we observe defects in *hox1-4* gene expression in *moz* mutants. Three pieces of evidence suggest that Moz functions similarly to trithrorax (trxG) factors in regulating maintenance of Hox gene expression, as we discuss below.

First, we do not detect changes in initiation of Hox gene expression in the hindbrain of *moz* mutants. By later stages, graded reduction of most *hox1-4* expression domains in the CNS domains is apparent. Defects in Hox gene maintenance, but not initiation, are hallmarks of *trx* mutants in *Drosophila* (Breen and Harte, 1993) and mouse (Yu et al., 1998). Loss of Hox group 1 or 2 gene function in zebrafish or in mice can cause severe homeotic neuronal transformations in the hindbrain and motor axon pathfinding defects (McClintock et al., 2002; Cooper et al., 2003; Studer et al., 1996; Gavalas et al., 1997; Gavalas et al., 1998; Gavalas et al., 2003; Rossel and Capecchi, 1999; Gendron-Maguire et al., 1993; Rijli et al., 1993). Supporting a role for *moz* in maintenance of Hox expression in the hindbrain, we find that early neuronal specification in the hindbrain and axonal trajectories in the head periphery are approximately normal in *moz* mutants. The only consistent neuronal defect we are able to detect in *moz* mutants is the disruption of facial motor neuron migration. This phenotype may be consistent with the defect in maintenance of *hoxb1a* expression in *moz* mutants, as loss of *hoxb1a* in zebrafish or *Hoxb1* in mice causes a similar defect (McClintock et al., 2002; Studer et al., 1996). In the mouse *Mll* (*trx*) mutant, cranial ganglia are condensed and fail to innervate the pharyngeal arches (Yu et al., 1998), but more specific neuronal defects have not been reported and MLL mutant zebrafish have not been described.

Second, Moz has a HAT domain, which for human MOZ has

been demonstrated to have HAT activity (Champagne et al., 2001), and HAT activity has been associated with trxG factors (Petruk et al., 2001; Milne et al., 2002). Furthermore, HAT activity is required for Moz function, as treatment with a histone deacetylase inhibitor rescues many aspects of the *moz* mutant phenotype.

Third, we find that *moz* mutant homeosis and Hox maintenance defects are rescued by TSA, and TSA has been shown to rescue defects caused by *trx*G mutations in *Drosophila* (Sollars et al., 2003) and human cells (Milne et al., 2002). Why does inhibition of histone deacetylase activity rescue a putative decrease of histone acetylation? It seems likely that the transcriptional on or off state of Hox genes is maintained through a balance of chromatin modification activities, including histone acetylation by *trx*G factors and histone deacetylation by *Polycomb* group (*Pc*G) factors (Milne et al., 2002) (reviewed by Francis and Kingston, 2001; Simon and Tamkun, 2002). In support of this idea, *trx*G and *Pc*G factors are antagonistic for proper Hox expression. For example, homeotic axial transformations and Hox expression defects of *Mll*-deficient mice and *Bmi1*-deficient mice are rescued when function of both genes is removed (Hanson et al., 1999; Yu et al., 1995; Yu et al., 1998). We do not yet know whether Moz directly acetylates histones associated with Hox regulatory regions. Western analyses show no detectable decrease of acetylated histone H4 levels in *moz* mutants compared with wild-type siblings (L.M., unpublished). We might expect to see rhombomere- or arch-specific defects in acetylated histone H4 levels at specific Hox genes, but at the present time this is very difficult to test.

Taken together, these findings implicate Moz as a trxG factor. *trx*G genes have been genetically defined as suppressors of *Pc*G mutant phenotypes (reviewed by Kennison, 1995). Further studies demonstrating genetic interactions between *moz* and *Pc*G genes would provide firm support for *moz* as a *trx*G gene.

One interesting aspect of Hox regulation that has emerged from our analysis of *moz* mutants is that in general, there appears to be a gradient effect of Moz activity within a Hox complex. We find that the *hox1-4* requirement for Moz activity ranges from strong for group 1 to weak for group 4, while group 5 and 6 Hox genes show no Moz requirement. We see this gradient effect on similar paralogs, where they have segmental domains in hindbrain and CNC, but we do not see a *moz* requirement for *hoxa1a* expression, even though *moz* appears to be expressed ubiquitously throughout the head. Our findings suggest that Moz activity plays a global role in Hox locus regulation, possibly through HAT activity. MYST family HAT activity has been shown to have a chromosomal gradient of transcription control in yeast (Kimura et al., 2002). Whether a Moz-mediated gradient of histone acetylation exists across group 1-5 genes in Hox clusters remains to be determined.

moz is required for late but not early patterning of head musculature

Our data suggest that at times when severe *hox2*, *bapx1* and *gsc* expression defects are present in postmigratory hyoid CNC of *moz* mutants, head mesodermal patterning appears unaffected. *eng2*, with *eng3* the only segmentally restricted head mesodermal marker that we know of (Ekker et al., 1992; Hatta et al., 1990), appears appropriately confined to the first

arch dorsal muscle core (constrictor dorsalis) of *moz* mutants. Likewise, the early *myod* expression pattern, which labels all proposed arch myogenic cores (see Kimmel et al., 2001b), appears normal in *moz* mutants. The absence of *eng2* duplication or *myod* pattern disruption could be due to residual *hox2* activity in *moz* mutants. Alternatively, *moz* and *hox2* genes could play no role in restricting *eng* expression to the first arch or setting up the pattern of *myod*-expressing myogenic cores. The homeotic late muscle pattern seen in *moz* mutants perhaps results from transformed CNC-derived connective tissue, which has been shown to pattern paraxial-mesodermally derived and somitic-derived myocytes (Noden, 1983a; Noden, 1983b; Noden, 1986).

Dramatic changes in CNC expression of *bapx1* and *gsc* prefigure the *moz* mutant phenotype

In stark contrast to the apparently normal early patterning of *moz* mutant mesoderm, endoderm and surface ectoderm, expression of two known *hox2* target genes, *bapx1* and *goosecoid* (*gsc*), is radically perturbed in postmigratory CNC of *moz* mutant second arch primordia.

Within postmigratory CNC, *bapx1* expression is confined to a patch of intermediate first arch mesenchyme which appears to prefigure the jaw joint (Miller et al., 2003). We previously identified *edn1* and *hand2* (*dHAND*) as positive and negative regulators, respectively, of *bapx1* expression. *bapx1* expression spreads ventrally in *hand2* mutants (Miller et al., 2003). We report that *moz* and *hox2* genes also contribute to positioning *bapx1* to the jaw joint, although these genes prevent *bapx1* from being expressed in an intermediate domain of the hyoid arch. Thus, *bapx1* integrates positional information from both the DV (*edn1*, *hand2*) and AP axes (*moz*, *hox2*) to achieve its jaw-joint-restricted expression. Furthermore, as an aspect of the *moz* mutant homeotic pattern (the jaw joint) requires *bapx1*, these results identify *bapx1* as a crucial downstream effector contributing to the homeotic transformation.

Microarray comparisons of gene expression in the second arches of wild-type and *Hoxa2* mutant mice revealed *Pitx1* to be upregulated in the *Hoxa2* mutant second pharyngeal arch primordial (Bobola et al., 2003), similar to what we report here for *bapx1*. These authors report finding no confirmed gene that is downregulated in *Hoxa2* mutant second arches, and suggest that *Hoxa2*-mediated segmental identity in the second arch might largely involve repression of the first arch program. Although microarray analyses promise to provide a global view of overall changes in gene expression in *Hoxa2* mutant arches, our demonstration of spatially shifted *gsc* expression highlights the need to also analyze potential spatial reorganization of affected genes.

In the mouse, *gsc* expression is spatially restricted within first and second arch CNC (Gaunt et al., 1993). Although *gsc* is required for specific aspects of mouse craniofacial development, defects in first, but not second, arch derivatives were reported (Rivera-Perez et al., 1995; Yamada et al., 1995). In both fruitflies and vertebrates, *gsc* functions as a transcriptional repressor (Danilov et al., 1998; Ferreiro et al., 1998; Mailhos et al., 1998; Latinkic and Smith, 1999; Yao and Kessler, 2001), although precedent exists for *gsc* positively regulating target genes (*frzb*) (Yasuo and Lemaire, 2001). The identity of *gsc* target genes and the nature of their regulation in the pharyngeal arches remains to be determined. *bapx1* and

gsc are expressed in strikingly complementary patterns in the first two arches (compare Fig. 9A-C with Fig. 10A-C), suggesting one might repress expression of the other. Our previous report that in *hand2* mutant zebrafish ventral first arch expression of *gsc* is lost, while *bapx1* expression expands ectopically into this domain (Miller et al., 2003), is consistent with *gsc* repressing *bapx1* arch expression.

The inverted *gsc* expression domain in the early second arch primordia of *moz* mutants suggests reorganization of the fate map at an early prechondrogenic stage has occurred. This model is consistent with our finding that *moz* mutant prechondrogenic condensations are mispositioned and the finding that in the mouse *Hoxa2* mutant, chondrogenesis is induced in different regions of the arch than in wild types (Kanzler et al., 1998). This latter study additionally showed that transgenically driving *Sox9* expression in the *Hoxa2* domain partially phenocopied the *Hoxa2* mutant phenotype. Furthermore, transgenically driving *Hoxa2* with an *Msx2* promoter resulted in loss of cranial bones, suggesting *Hoxa2* represses both cartilage and bone formation (Kanzler et al., 1998). Our *bapx1* and *gsc* expression data suggests that *moz* and *hox2* affect patterning within the second arch primordia long before cartilage or bone differentiation occurs.

Perhaps *gsc* expression labels chondrogenic cells and these cells shift medial in the early CNC cylinder. Alternatively, *gsc* expression could label non-chondrogenic cells. Although the first model is more consistent with the demonstrated cell-autonomous function of *gsc* in mice (Rivera-Perez et al., 1999), the latter is more consistent with the *moz* mutant phenotype, in which the lateral end of the duplicated lower jaw cartilage fuses laterally with the lower jaw near the jaw joint. In mice, although *gsc* was found to be cell autonomous, *gsc*-null cells in the presence of wild-type cells could contribute to the condensation of the tympanic bone, a bone that never forms in *gsc* mutants (Rivera-Perez et al., 1995; Rivera-Perez et al., 1999; Yamada et al., 1995). However, these *gsc*-null cells were not maintained (Rivera-Perez et al., 1999). Exogenous *gsc* can induce neighboring cells to form a secondary axis, suggesting in some contexts, Gsc can have non cell-autonomous functions (Cho et al., 1991; Niehrs et al., 1993).

A central mystery remaining is why the duplication in *moz* or *hox2*-deficient animals is mirror image. At the time the *gsc* expression defect appears, *hoxa2* expression appears to mark all hyoid postmigratory CNC. Thus, the spatially complex *gsc* defect in hox2-injected animals is hard to reconcile with a model in which *hox2* genes simply positively regulate *gsc*. The *gsc* expression defect is also hard to reconcile with a model in which *hox2* genes modify responsiveness of second arch CNC to a single cue emanating from the arch 1/2 boundary (Rijli et al., 1993). We propose a modified version of the model of Rijli et al., in which *hox2* modifies the responsiveness of hyoid CNC to multiple environmental signals. The mediolateral inversion of *gsc* could be explained if *hox2* genes conferred responsiveness of second arch CNC to a lateral surface ectodermal signal cue to activate *gsc* while repressing responsiveness to a medial endodermal cue that normally repressed *gsc* expression. Continued forward genetic screens in zebrafish could reveal components of these putative signaling pathways that underlie segmental identity in the pharyngeal arches.

References

Aguiar, R. C. T., Chase, A., Coulthard, S., Macdonald, D. H. C., Carapeti, M., Reiter, A., Sohal, J., Lennard, A., Goldman, J. M. and Cross, N. C. P. (1997). Abnormalities of chromosome band 8p11 in leukemia: two clinical syndromes can be distinguished on the basis of MOZ involvement. *Blood* **90**, 3130-3135.

Amemiya, C. T. and Zon, L. I. (1999). Generation of a zebrafish P1 artificial chromosome library. *Genomics* **58**, 211-213.

Amores, A., Force, A., Yan, Y.-L., Joly, L., Amemiya, C., Fritz, A., Ho, R., Langeland, J., Prince, V., Wang, Y.-L. et al. (1998). Zebrafish *hox* clusters and vertebrate genome evolution. *Science* **282**, 1711-1714.

Armstrong, S. A., Staunton, J. E., Silverman, L. B., Pieters, R., den Boer, M. L., Minden, M. D., Sallan, S. E., Lander, E. S., Golub, T. R. and Korsmeyer, S. J. (2002). MLL translocations specify a distinct gene expression profile that distinguishes a unique leukemia. *Nat. Genet.* **30**, 41-47.

Barrow, J. R. and Capecchi, M. R. (1999). Compensatory defects associated with mutations in *Hoxa1* restore normal palatogenesis to *Hoxa2* mutants. *Development* **126**, 5011-5026.

Bobola, N., Carapuco, M., Ohnemus, S., Kanzler, B., Leibbrandt, A., Neubuser, A., Drouin, J. and Mallo, M. (2003). Mesenchymal patterning by *Hoxa2* requires blocking Fgf-dependent activation of *Ptx1*. *Development* **130**, 3403-3414.

Borrow, J., Stanton, V. P., Jr, Andresen, J. M., Becher, R., Behm, F. G., Chaganti, R. S., Civin, C. I., Disteche, C., Dube, I., Frischauf, A. M. et al. (1996). The translocation t(8;16)(p11;p13) of acute myeloid leukaemia fuses a putative acetyltransferase to the CREB-binding protein. *Nat. Genet.* **14**, 33-41.

Breen, T. R. and Harte, P. J. (1993). Trithorax regulates multiple homeotic genes in the bithorax and Antennapedia complexes and exerts different tissue-specific, parasegment-specific and promoter-specific effects on each. *Development* **117**, 119-134.

Brown, L. A., Amores, A., Schilling, T. F., Jowett, T., Baert, J. L., de Launoit, Y. and Sharrocks, A. D. (1998). Molecular characterization of the zebrafish PEA3 ETS-domain transcription factor. *Oncogene* **17**, 93-104.

Carapeti, M., Aguiar, R. C. T., Goldman, J. M. and Cross, N. C. P. (1998). A novel fusion between *MOZ* and the nuclear receptor coactivator *TIF2* in acute myeloid leukemia. *Blood* **91**, 3127-3133.

Carapeti, M., Aguiar, R. C. T., Watmore, A. E., Goldman, J. M. and Cross, N. C. P. (1999). Consistent fusion of *MOZ* and *TIF2* in AML with inv(8)(p11p13). *Cancer Genet. Cytogenet.* **113**, 70-72.

Chaffanet, M., Gressin, L., Preudhomme, C., Soenen-Cornu, V., Birnbaum, D. and Pebusque, M.-J. (2000). MOZ is fused to p300 in an acute monocytic leukemia with t(8;22). *Genes Chromosomes Cancer* **28**, 138-144.

Champagne, N., Bertos, N. R., Pelletier, N., Wang, A. H., Vezmar, M., Yang, Y., Heng, H. H. and Yang, X.-J. (1999). Identification of a human histone acetyltransferase related to monocytic leukemia zinc finger protein. *J. Biol. Chem.* **274**, 28528-28536.

Champagne, N., Pelletier N. and Yang, X. J. (2001). The monocytic leukemia zinc finger protein MOZ is a histone acetyltransferase. *Oncogene* **20**, 404-409.

Chandrasekhar, A., Moens, C. B., Warren, J. T., Jr, Kimmel, C. B. and Kuwada, J. Y. (1997). Development of branchiomotor neurons in zebrafish. *Development* **124**, 2633-2644.

Cho, K. W. Y., Blumberg, B., Steinbesser, H. and de Robertis, E. M. (1991). Molecular nature of Spemann's organizer: the role of the *Xenopus* homeobox gene *Goosecoid*. *Cell* **67**, 1111-1120.

Collas, P., Liang, M.-R., Vincent, M. and Alestrom, P. (1999). Active transgenes in zebrafish are enriched in acetylated histone H4 and dynamically associate with RNA Pol II and splicing complexes. *J. Cell. Sci.* **112**, 1045-1054.

Cooper, K. L., Leisenring, W. M. and Moens, C. B. (2003). Autonomous and nonautonomous functions for Hox/Pbx in branchiomotor neuron development. *Dev. Biol.* **253**, 200-213.

Couly, G., Creuzet, S., Bennaceur, S., Vincent, C. and le Douarin, N. M. (2002). Interactions between Hox-negative cephalic neural crest cells and the foregut endoderm in patterning the facial skeleton in the vertebrate head. *Development* **129**, 1061-1073.

Danilov, V., Blum, M., Schweickert, A., Campione, M. and Steinbesser, H. (1998). Negative autoregulation of the organizer-specific homeobox gene *goosecoid*. *J. Biol. Chem.* **273**, 627-635.

de Beer, G. R. (1937). *The Development of the Vertebrate Skull*. Oxford: Oxford University Press.

Edgeworth, F. H. (1935). *The Cranial Muscles of Vertebrates*. Cambridge: Cambridge University Press.

Ekker, M., Wegner, J., Akimenko, M. A. and Westerfield, M. (1992). Coordinate embryonic expression of three zebrafish *engrailed* genes. *Development* **116**, 1001-1010.

Epperlein, H. H. (1974). The ectomesenchymal-endodermal interaction-system (EEIS) of *Trituris alpestris* in tissue culture. I. Observations on attachment, migration, and differentiation of neural crest cells. *Differentialtion* **2**, 151-168.

Ernst, P., Wang, J. and Korsmeyer, S. J. (2002). The role of *MLL* in hematopoiesis and leukemia. *Curr. Opin. Hemat.* **9**, 282-287.

Essner, J. J., Branford, W. W., Zhang, J. and Yost, H. J. (2000). Mesendoderm and left-right brain, heart and gut development are differentially regulated by pitx2 isoforms. *Development* **127**, 1081-1093.

Ferreiro, B., Artinger, M., Cho, K. W. Y. and Niehrs, C. (1998). Antimorphic *goosecoids*. *Development* **125**, 1347-1359.

Francis, N. J. and Kingston, R. E. (2001). Mechanisms of transcriptional memory. *Nat. Rev. Mol. Cell Biol.* **2**, 409-421.

Gaunt, S. J., Blum, M. and de Robertis, E. M. (1993). Expression of the mouse *Goosecoid* gene during mid-embryogenesis may mark mesenchymal cell lineages in the developing head, limbs, and body wall. *Development* **117**, 769-778.

Gavalas, A., Davenne, M., Lumsden, A., Chambon, P. and Rijli, F. M. (1997). Role of *Hoxa-2* in axon pathfinding and rostral hindbrain patterning. *Development* **124**, 3693-3702.

Gavalas, A., Studer, M., Lumsden, A., Rijli, F. M., Krumlauf, R. and Chambon, P. (1998). *Hoxa1* and *Hoxb1* synergize in patterning the hindbrain, cranial nerves, and second pharyngeal arch. *Development* **125**, 1123-1136.

Gavalas, A., Trainor, P., Ariza-McNaughton, L. and Krumlauf, R. (2001). Synergy between *Hoxa1* and *Hoxb1*: the relationship between arch patterning and the generation of cranial neural crest. *Development* **128**, 3017-3027.

Gavalas, A., Ruhrberg, C., Livet, J., Henderson, C. E. and Krumlauf, R. (2003). Neuronal defects in the hindbrain of *Hoxa1*, *Hoxb1*, and *Hoxb2* mutants reflect regulatory interactions among these Hox genes. *Development* **130**, 5663-5679.

Gendron-Maguire, M., Mallo, M., Zhang, M. and Gridley, T. (1993). *Hoxa-2* mutant mice exhibit homeotic transformation of skeletal elements derived from cranial neural crest. *Cell* **75**, 1317-1331.

Goddard, J. M., Rossel, M., Manley, N. M. and Capecchi, M. R. (1996). Mice with targeted disruption of *Hoxb-1* fail to form the motor nucleus of the VIIth nerve. *Development* **122**, 3217-3228.

Grammatopoulos, G. A., Bell, E., Toole, L., Lumsden, A. and Tucker, A. S. (2000). Homeotic transformation of branchial arch identity after *Hoxa2* overexpression. *Development* **127**, 5355-5365.

Hanson, R. D., Hess, J. L., Yu, B. D., Ernst, P., van Lohuizen, M., Berns, A., van der Lugt, N. M. T., Shashikant, C. S., Ruddle, F. H., Seto, M. et al. (1999). Mammalian *Trithorax* and *Polycomb*-group homologues are antagonistic regulators of homeotic development. *Proc. Natl. Acad. Sci. USA* **96**, 14372-14377.

Hatta, K., Schilling, T. F., BreMiller, R. A. and Kimmel, C. B. (1990). Specification of jaw muscle identity in zebrafish: correlation with *engrailed*-homeoprotein expression. *Science* **250**, 802-805.

Higashijima, S., Hotta, Y. and Okamoto, H. (2000). Visualization of cranial motor neurons in live transgenic zebrafish expressing green fluorescent protein under the control of the *Islet-1* promoter/enhancer. *J. Neurosci.* **20**, 206-218.

Hunt, P., Gulisano, M., Cook, M., Sham, M.-H., Faiella, A., Wilkinson, D., Boncinelli, E. and Krumlauf, R. (1991). A distinct *Hox* code for the branchial region of the vertebrate head. *Nature* **353**, 861-864.

Hunter, M. P. and Prince, V. E. (2002). Zebrafish Hox paralogue group 2 genes function redundantly as selector genes to pattern the second pharyngeal arch. *Dev. Biol.* **247**, 367-389.

Jerome, L. A. and Papaioannou, V. E. (2001). DiGeorge syndrome phenotype in mice mutant for the T-box gene, Tbx1. *Nat. Genet.* **27**, 286-291.

Kanzler, B., Kuschert, S. J., Liu, Y.-H. and Mallo, M. (1998). *Hoxa-2* restricts the chondrogenic domain and inhibits bone formation during development of the branchial area. *Development* **125**, 2587-2597.

Kennison, J. A. (1995). The Polycomb and trithorax group proteins of Drosophila: trans-regulators of homeotic gene function. *Annu. Rev. Genet.* **29**, 289-303.

Kimmel, C. B., Ballard, W. W., Kimmel, S. R., Ullmann, B. and Schilling, T. F. (1995). Stages of embryonic development of the zebrafish. *Dev. Dyn.* **203**, 253-310.

Kimmel, C. B., Miller, C. T., Kruze, G., Ullmann, B., BreMiller, R. A., Larison, K. D. and Snyder, H. C. (1998). The shaping of pharyngeal cartilages during early development of the zebrafish. *Dev. Biol.* **203**, 245-263.

Kimmel, C. B., Miller, C. T. and Moens, C. B. (2001a). Specification and morphogenesis of the larval zebrafish head skeleton. *Dev. Biol.* **233**, 239-257.

Kimmel, C. B., Miller, C. T. and Keynes, R. J. (2001b). Neural crest patterning and evolution of the jaw. *J. Anat.* **199**, 105-120.

Kimmel, C. B., Ullmann, B., Walker, M., Miller, C. T. and Crump, J. G. (2003). Endothelin-1 mediated regulation of pharyngeal bone development in zebrafish. *Development* **130**, 1339-1351.

Kimura, A., Umehara, T. and Horikoshi, M. (2002). Chromosomal gradient of histone acetylation established by Sas2p and Sir2p functions as a shield against gene silencing. *Nat. Genet.* **32**, 370-377.

Kitabayashi, I., Aikawa, Y., Nguyen, L. A., Yokoyama, A. and Ohki, M. (2001a). Activation of AML1-mediated transcription by MOZ and inhibition by the MOZ-CBP fusion protein. *EMBO J.* **20**, 7184-7196.

Kitabayashi, I., Aikawa, Y., Yokoyama, A., Hosoda, F., Nagai, M., Kakazu, N., Abe, T. and Ohki, M. (2001b). Fusion of MOZ and p300 histone acetyltransferases in acute monocytic leukemia with a t(8;22)(p11;q13) chromosome translocation. *Leukemia* **15**, 89-94.

Knight, R. D., Nair, S., Nelson, S. S., Afshar, A., Javidan, Y., Geisler, R., Rauch, J.-G. and Schilling, T. F. (2003). *lockjaw* encodes a zebrafish *tfap2a* required for early neural crest development. *Development* **130**, 5755-5768.

Köntges, G. and Lumsden, A. (1996). Rhombencephalic neural crest segmentation is preserved throughout craniofacial ontogeny. *Development* **122**, 3229-3242.

Krauss, S., Concordet, J.-P. and Ingham, P. W. (1993). A functionally conserved homolog of the Drosophila segment polarity gene *hh* is expressed in tissues with polarizing activity in zebrafish embryos. *Cell* **75**, 1431-1444.

Kroon, E., Krosl, J., Thorsteinsdottir, U., Baban, S., Buchberg, A. M. and Sauvageau, G. (1998). *Hoxa9* transforms primary bone marrow cells through specific collaboration with *Meis1a* but not *Pbx1b*. *EMBO J.* **17**, 3714-3725.

Kurihara, Y., Kurihara, H., Suzuki, H., Kodama, T., Maemura, K., Nagai, R., Oda, H., Kuwaki, T., Cao, W. H., Kamada, N. et al. (1994). Elevated blood pressure and craniofacial abnormalities in mice deficient in endothelin-1. *Nature* **368**, 703-710.

Latinkic, B. V. and Smith, J. C. (1999). Goosecoid and mix.1 repress Brachyury expression and are required for head formation in Xenopus. *Development* **126**, 1769-1779.

LeDouarin, N. M. and Jotereau, F. V. (1975). Tracing of cells of the avian thymus through embryonic life in interspecific chimeras. *J. Exp. Med.* **142**, 17-40.

Liang, J., Prouty, L., Willians, B. J., Dayton, M. A. and Blanchard, K. L. (1998). Acute mixed lineage leukemia with an inv(8)(p11q13) resulting in fusion of genes for MOZ and TIF2. *Blood* **92**, 2118-2122.

Look, A. (1997). Oncogenic transcription factors in the human acute leukemias. *Science* **278**, 1059-1064.

Maconochie, M., Krishnamurthy, R., Nonchev, S., Meier, P., Manzanares, M., Mitchell, P. J. and Krumlauf, R. (1999). Regulation of *Hoxa2* in

cranial neural crest cells involves members of the *AP-2* family. *Development* **126**, 1483-1494.

Magli, M. C., Largman, C. and Lawrence, H. J. (1997). Effects of HOX homeobox genes in blood cell differentiation. *J. Cell Physiol.* **173**, 168-177.

Mailhos, C., Andre, S., Mollereau, B., Goriely, A., Hemmati-Brivanlou-A. and Desplan, C. (1998). Drosophila Goosecoid requires a conserved heptapeptide for repression of paired-class homeoprotein activators. *Development* **125**, 937-947.

Manley, N. R. and Capecchi, M. R. (1995). The role of *Hoxa-3* in mouse thymus and thyroid development. *Development* **121**, 1989-2003.

Manley, N. R. and Capecchi, M. R. (1998). *Hox* group paralogs regulate the development and migration of the thymus, thyroid, and parathyroid glands. *Dev. Biol.* **195**, 1-15.

Maves, L., Jackman, W. and Kimmel, C. B. (2002). FGF3 and FGF8 mediate a rhombomere 4 signaling activity in the zebrafish hindbrain. *Development* **129**, 3825-3837.

McClintock, J. M., Carlson, R., Mann, D. M. and Prince, V. E. (2001). Consequences of Hox gene duplication in the vertebrates: an investigation of the zebrafish Hox paralogue group 1 genes. *Development* **128**, 2471-2484.

McClintock, J. M., Kheirbek, M. A. and Prince, V. E. (2002). Knockdown of duplicated zebrafish *hoxb1* genes reveals distinct roles in hindbrain patterning and a novel mechanism of duplicate gene retention. *Development* **129**, 2339-2354.

McClintock, J. M., Jozefowicz, C., Assimacopoulos, S., Grove, E. A., Louvi, A. and Prince, V. E. (2003). Conserved expression of *Hoxa1* in neurons at the ventral forebrain/midbrain boundary of vertebrates. *Dev. Genes Evol.* **213**, 399-406.

Mendelson, B. (1986). Development of reticulospinal neurons of the zebrafish. I. Time of origin. *J. Comp. Neurol.* **251**, 160-171.

Miller, C. T., Schilling, T. F., Lee, K.-H., Parker, J. and Kimmel, C. B. (2000). *sucker* encodes a zebrafish Endothelin-1 required for ventral pharyngeal arch development. *Development* **127**, 3815-3828.

Miller, C. T. and Kimmel, C. B. (2001). Morpholino phenocopies of *endothelin 1* (*sucker*) and other anterior arch class mutations. *Genesis* **30**, 186-187.

Miller, C. T., Yelon, D., Stainier, D. Y. R. and Kimmel, C. B. (2003). Two *endothelin1* effectors, *hand2* and *bapx1,* pattern ventral pharyngeal cartilage and the jaw joint. *Development* **130**, 1353-1365.

Milne, T. A., Briggs, S. D., Brock, H. W., Martin, M. E., Gibbs, D., Allis, C. D. and Hess, J. L. (2002). MLL targets SET domain methyltransferase activity to *Hox* gene promoters. *Mol. Cell* **10**, 1107-1117.

Moens, C. B., Cordes, S. P., Giorgianni, M. W., Barsh, G. S. and Kimmel, C. B. (1998). Equivalence in the genetic control of hindbrain segmentation in fish and mouse. *Development* **125**, 381-391.

Neff, M. M., Neff, J. D., Chory, J. and Pepper, A. E. (1998). dCAPS, a simple technique for the genetic analysis of single nucleotide polymorphisms: experimental applications in *Arabidopsis thaliana* genetics. *Plant J.* **14**, 387-392.

Neuhauss, S. C., Solnica-Krezel, L., Schier, A. F., Zwartkruis, F., Stemple, D. L., Malicki, J., Abdelilah, S., Stainier, D. Y. and Driever, W. (1996). Mutations affecting craniofacial development in zebrafish. *Development* **123**, 357-367.

Niehrs, C., Keller, R., Cho, K. W. Y. and de Robertis, E. M. (1993). The homeobox gene *Goosecoid* controls cell migration in *Xenopus* embryos. *Cell* **72**, 491-503.

Noden, D. M. (1983a). The role of the neural crest in patterning of avian cranial skeletal, connective, and muscle tissues. *Dev. Biol.* **96**, 144-165.

Noden, D. M. (1983b). The embryonic origins of avian cephalic and cervical muscles and associated connective tissues. *Am. J. Anat.* **168**, 257-276.

Noden, D. M. (1986). Patterning of avian craniofacial muscles. *Dev. Biol.* **116**, 347-356.

Ohnemus, S., Bobola, N., Kanzler, B. and Mallo, M. (2001). Different levels of *Hoxa2* are required for particular developmental processes. *Mech. Dev.* **108**, 135-147.

Panagopoulos, I., Fioretos, T., Isaksson, M., Samuelsson, U., Billstrom, R., Strombeck, B., Mitelman, F. and Johansson, B. (2001). Fusion of the *MORF* and *CBP* genes in acute myeloid leukemia with the t(10;16)(q22;p13). *Hum. Mol. Gen.* **10**, 395-404.

Pasqualetti, M., Ori, M., Nardi, I. and Rijli, F. M. (2000). Ectopic *Hoxa2* induction after neural crest migration results in homeosis of jaw elements in *Xenopus*. *Development* **127**, 5367-5378.

Pelletier, N., Champagne, N., Stifani, S. and Yang, X.-J. (2002). MOZ and MORF histone acetyltransferases interact with the Runt-domain transcription factor Runx2. *Oncogene* **21**, 2729-2740.

Petruk, S., Sedkov, Y., Smith, S., Tillib, S., Kraevski, V., Nakamura, T., Canaani, E., Croce, C. M. and Mazo, A. (2001). Trithorax and dCBP acting in a complex to maintain expression of a homeotic gene. *Science* **294**, 1331-1334.

Piotrowski, T. and Nüsslein-Volhard, C. (2000). The endoderm plays an important role in patterning the segmented pharyngeal region in zebrafish (Danio rerio). *Dev. Biol.* **225**, 339-356.

Piotrowski, T., Schilling, T. F., Brand, M., Jiang, Y. J., Heisenberg, C. P., Beuchle, D., Grandel, H., van Eeden, F. J., Furutani-Seiki, M., Granato, M. et al. (1996). Jaw and branchial arch mutants in zebrafish II: anterior arches and cartilage differentiation. *Development* **123**, 345-356.

Piotrowski, T., Ahn, D.-G., Schilling, T. F., Nair, S., Ruvinsky, I., Geisler, R., Rauch, G.-J., Haffter, P., Zon, L. I., Zhou, Y. et al. (2003). The zebrafish *van gogh* mutation disrupts *tbx1*, which is involved in the DiGeorge deletion syndrome in humans. *Development* **130**, 5043-5052.

Pöpperl, H., Rikhof, H., Chang, H., Haffter, P., Kimmel, C. B. and Moens, C. B. (2000). *lazarus* is a novel *pbx* gene that globally mediates *hox* gene function in zebrafish. *Mol. Cell* **6**, 255-267.

Prince, V. E. and Lumsden, A. (1994). Hoxa-2 expression in normal and transposed rhombomeres: independent regulation in the neural tube and neural crest. *Development* **120**, 911-923.

Prince, V. E., Moens, C. B., Kimmel, C. B. and Ho, R. K. (1998). Zebrafish *hox* genes: expression in the hindbrain region of wild-type and mutants of the segmentation gene, *valentino*. *Development* **125**, 393-406.

Rijli, F. M., Mark, M., Lakkaraju, S., Dierich, A., Dolle, P. and Chambon, P. (1993). A homeotic transformation is generated in the rostral branchial region of the head by disruption of *Hoxa-2*, which acts as a selector gene. *Cell* **75**, 1333-1349.

Riley, B. B. and Grunwald, D. J. (1995). Efficient induction of point mutations allowing recovery of specific locus mutations in zebrafish. *Proc. Natl. Acad. Sci. USA* **92**, 5997-6001.

Rivera-Perez, J. A., Mallo, M., Gendron-Maguire, M., Gridley, T. and Behringer, R. R. (1995). *goosecoid* is not an essential component of the mouse gastrula organizer but is required for craniofacial and rib development. *Development* **121**, 3005-3012.

Rivera-Perez, J. A., Wakamiya, M. and Behringer, R. R. (1999). *Goosecoid* acts cell autonomously in mesenchyme-derived tissues during craniofacial development. *Development* **126**, 3811-3821.

Roehl, H. and Nüsslein-Volhard, C. (2001). Zebrafish *pea3* and *erm* are general targets of FGF8 signaling. *Curr. Biol.* **11**, 503-507.

Rossel, M. and Capecchi, M. R. (1999). Mice mutant for both *Hoxa1* and *Hoxb1* show extensive remodeling of the hindbrain and defects in craniofacial development. *Development* **126**, 5027-5040.

Rozovskaia, T., Feinstein, E., Mor, O., Foa, R., Blechman, J., Nakamura, T., Croce, C. M., Cimino, G. and Canaani, E. (2001). Upregulation of Meis1 and HoxA9 in acute lymphocytic leukemias with the t(4:11) abnormality. *Oncogene* **20**, 874-878.

Schilling, T. F. and Kimmel, C. B. (1997). Musculoskeletal patterning in the pharyngeal segments of the zebrafish embryo. *Development* **124**, 2945-2960.

Schilling, T. F., Piotrowski, T., Grandel, H., Brand, M., Heisenberg, C. P., Jiang, Y. J., Beuchle, D., Hammerschmidt, M., Kane, D. A., Mullins, M. C. et al. (1996a). Jaw and branchial arch mutants in zebrafish I: branchial arches. *Development* **123**, 329-344.

Schilling, T. F., Walker, C. and Kimmel, C. B. (1996b). The *chinless* mutation and neural crest interactions in zebrafish jaw development. *Development* **122**, 1417-1426.

Schorle, H., Meier, P., Buchert, M., Jaenisch, R. and Mitchell, P. J. (1996). Transcription factor AP-2 essential for cranial closure and craniofacial development. *Nature* **381**, 235-238.

Schulte-Merker, S., Hammerschmidt, M., Beuchle, D., Cho, K. W., de Robertis, E. M. and Nüsslein-Volhard, C. (1994). Expression of zebrafish *goosecoid* and *no tail* gene products in wild-type and mutant *no tail* embryos. *Development* **120**, 843-852.

Schweickert, A., Steinbeisser, H. and Blum, M. (2001). Differential gene expression of *Xenopus Pitx1*, *Pitx2b*, and *Pitx2c* during cement gland, stomodeum, and pituitary development. *Mech. Dev.* **107**, 191-194.

Selleri, L., Depew, M. J., Jacobs, Y., Chanda, S. K., Tsang, K. Y., Cheah, K. S. E., Rubenstein, J. L. R., O'Gorman, S. and Cleary, M. L. (2001). Requirement for *Pbx1* in skeletal patterning and programming chondrocyte proliferation and differentiation. *Development* **128**, 3543-3557.

Simon, J. A. and Tamkun, J. W. (2002). Programming off and on states in chromatin: mechanisms of Polycomb and trithorax group complexes. *Curr. Opin. Genet. Dev.* **12**, 210-218.

Sollars, V., Lu, X., Xiao, L., Wang, X., Garfinkel, M. D. and Ruden, D. M.

(2003). Evidence for an epigenetic mechanism by which Hsp90 acts as a capacitor for morphological evolution. *Nat. Genet.* **33**, 70-74.

Solnica-Krezel, L., Schier, A. F. and Driever, W. (1994). Efficient recovery of ENU-induced mutations from the zebrafish germline. *Genetics* **136**, 1401-1420.

Streisinger, G., Walker, C., Dower, N., Knauber, D. and Singer, F. (1981). Production of clones of homozygous diploid zebra fish (*Brachydanio rerio*). *Nature* **291**, 293-296.

Studer, M., Lumsden, A., Ariza-McNaughton, L., Rijli, F. M., Chambon, P. and Krumlauf, R. (1996). Altered segmental identity and abnormal migration of motor neurons in mice lacking *Hoxb-1*. *Nature* **384**, 630-634.

Thisse, C., Thisse, B., Schilling, T. F. and Postlethwait, J. H. (1993). Structure of the zebrafish *snail1* gene and its expression in wild-type, *spadetail* and *no tail* mutant embryos. *Development* **119**, 1203-1215.

Thomas, T., Voss, A. K., Chowdhury, K. and Gruss, P. (2000). Querkopf, a MYST family histone acetyltransferase, is required for normal cerebral cortex development. *Development* **127**, 2537-2548.

Trainor, P. and Krumlauf, R. (2000). Plasticity in mouse neural crest cells reveals a new patterning role for cranial mesoderm. *Nat. Cell Biol.* **2**, 96-102.

Trainor, P., Ariza-McNaughton, L. and Krumlauf, R. (2002). Role of the isthmus and FGFs in resolving the paradox of neural crest plasticity and prepatterning. *Science* **295**, 1288-1291.

Tyler, M. S. and Hall, B. K. (1977). Epithelial influences on skeletogenesis in the mandible of the embryonic chick. *Anat. Rec.* **188**, 229-239.

Veitch, E., Begbie, J., Schilling, T. F., Smith, M. M. and Graham, A. (1999). Pharyngeal arch patterning in the absence of neural crest. *Curr. Biol.* **9**, 1481-1484.

Wall, N. A. and Hogan, B. L. M. (1995). Expression of bone morphogenetic protein-4 (BMP-4), bone morphogenetic protein-7 (BMP-7), fibroblast growth factor-8 (FGF-8) and sonic hedgehog (SHH) during branchial arch development in the chick. *Mech. Dev.* **53**, 383-392.

Weinberg, E. S., Allende, M. L., Kelly, C. S., Abdelhamid, A., Murakami, T., Andermann, P., Doerre, O. G., Grunwald, D. J. and Riggleman, B. (1996). Developmental regulation of zebrafish MyoD in wild-type, no tail and spadetail embryos. *Development* **122**, 271-280.

Westerfield, M. (1995) *The Zebrafish Book.* Eugene, OR: University of Oregon Press.

Willett, C. E., Zapata, A. G., Hopkins, N. and Steiner, L. A. (1997). Expression of zebrafish *rag* genes during early development identifies the thymus. *Dev. Biol.* **182**, 331-341.

Yamada, G., Mansouri, A., Torres, M., Stuart, E. T., Blum, M., Schultz, M., de Robertis, E. M. and Gruss, P. (1995). Targeted mutation of the murine *goosecoid* gene results in craniofacial defects and neonatal death. *Development* **121**, 2917-2922.

Yan, Y.-L., Miller, C. T., Nissen, R. M., Singer, A., Liu, D., Kirn, A., Draper, B., Willoughby, J., Morcos, P. A., Amsterdam, A. et al. (2002). A zebrafish *sox9* gene required for cartilage morphogenesis. *Development* **129**, 5065-5079.

Yao, J. and Kessler, D. S. (2001). Goosecoid promotes head organizer activity by direct repression of Xwnt8 in Spemann's organizer. *Development* **128**, 2975-2987.

Yasuo, H. and Lemaire, P. (2001). Role of Goosecoid, Xnot, and Wnt antagonists in the maintenance of the notochord genetic programme in *Xenopus* gastrulae. *Development* **128**, 3783-3793.

Yeoh, E. J., Ross, M. E., Shurtleff, S. A., Williams, W. K., Patel, D., Mahfouz, R., Behm, F. G., Raimondi, S. C., Relling, M. V., Patel, A. et al. (2002). Classification, subtype discovery, and prediction of outcome in pediatric acute lymphoblastic leukemia by gene expression profiling. *Cancer Cell* **1**, 133-143.

Yu, B. D., Hess, J. L., Horning, S. E., Brown, G. A. and Korsmeyer, S. J. (1995). Altered Hox expression and segmental identity in Mll-mutant mice. *Nature* **378**, 505-508.

Yu, B. D., Hanson, R. D., Hess, J. L., Horning, S. E. and Korsmeyer, S. J. (1998). MLL, a mammalian *trithorax*-group gene, functions as a transcriptional maintenance factor in morphogenesis. *Proc. Natl. Acad. Sci. USA* **95**, 10632-10636.

Zhang, J., Hagopian-Donaldson, S., Serbedzija, G., Elsemore, J., Plehn-Dujowich, D., McMahon, A. P., Flavell, R. A. and Williams, T. (1996). Neural tube, skeletal and body wall defects in mice lacking transcription factor AP-2. *Nature* **381**, 238-241.